Research Square

Preprints are preliminary reports that have not undergone peer review.
They should not be considered conclusive, used to inform clinical practice,
or referenced by the media as validated information.

Site Response Characterization Investigation of Kathmandu Valley by HVSR Ambient Noise Analysis

Khemraj Pokharel

078phce109.khemraj@pcampus.edu.np

Tribhuvan University Institute of Engineering Pulchowk Campus: Tribhuvan University Institute of Engineering https://orcid.org/0009-0005-2725-0063

Hari Ram Parajuli

Tribhuvan University Institute of Engineering Pulchowk Campus: Tribhuvan University Institute of Engineering https://orcid.org/0009-0001-0139-0691

Ram Chandra Tiwari

Tribhuvan University Institute of Engineering Pulchowk Campus: Tribhuvan University Institute of Engineering

Research Article

Keywords:

Posted Date: November 3rd, 2026

DOI: https://doi.org/10.21203/rs.3.rs-10963638/v1

License: This work is licensed under a Creative Commons Attribution 4.0 International License.
Read Full License

Site Response Characterization Investigation of Kathmandu Valley by HVSR Ambient Noise Analysis

Khemraj Pokharel[a], *Hari Ram Parajuli*[b*], *Ram Chandra Tiwari*[c]

[a]PhD Scholar, Department of Civil Engineering, IOE Pulchowk Campus, Tribhuvan University, Kathmandu, Nepal;
[b*]Associate Professor, Department of Civil Engineering, IOE Pulchowk Campus, Tribhuvan University, Kathmandu, Nepal;
[c]Assistant Professor, Department of Civil Engineering, IOE Pulchowk Campus, Tribhuvan University, Kathmandu, Nepal.

***Corresponding Author:** hariparajuli@ioe.edu.np

ABSTRACT:

Microtremor measurements for the seismic microzonation of the Kathmandu Valley were conducted at 75 stations spread across a 500 m × 500 m grid in the current study. The amplification factor (Ap) and predominant frequency (Fp) of the surface soils are estimated using the Horizontal-to-Vertical Spectral Ratio (HVSR) approach. The findings indicate that Fp ranges from 0.7 to 5.45 Hz and Ap spans from 1.0 to 6.2 Hz throughout the valley. Higher frequencies are found on the basin borders and in the southern regions where shallower stiff deposits predominate, whereas lower frequencies are found in the northern regions with thick lacustrine sediments. The soil classification revealed 1.3\% very soft, 24\% soft, and 74.67\% stiff soils based on the fp. Bhaktapur (B-21) and Lalitpur (L-24), two highly populated locations with a fragile building stock, were found to have significant amplification sites, suggesting a high potential for soil-structure resonance. The stable zones below 1.5 Hz showed low amplification, while Bhaktapur (4.39 Hz) and Lalitpur (5.45 Hz) showed the highest amplification, suggesting potential liquefaction or slope instability risks that need to be verified by geotechnical data and shear-wave velocity profiling. By facilitating neighborhood-level hazard assessments and offering helpful data to architects, engineers, and urban planners, the 500 m grid spacing greatly increased the microzonation resolution. Despite its limitations, such as the inability to completely quantify soil dynamics, the absence of two or three-dimensional basin modeling, and ambient noise interference, the HVSR approach is a reasonable starting point for valley-wide microzonation. To validate risk zones and improve engineering applications for seismic hazard assessment and catastrophe mitigation, future research should include these findings with MASW surveys, borehole Vs30 data, and numerical basin response models. The findings show that macro-scale danger maps often oversimplify the highly varied soil in the Kathmandu Valley.

Keywords: Seismic microzonation, Microtremor (HVSR), Predominant frequency, Am-plification factor, Earthquake hazard

1 Introduction

The Kathmandu Valley is among the most seismically vulnerable areas in the Himalayas because of the tectonic setting, rapid urbanisation and unique geological configuration (Acharya et al., 2021). The interaction between the Indian and Eurasian plates has resulted in a complex network of faults, which have been responsible for frequent and large earthquakes in 1934, 1966, 1980, 1988 and 2015 (Pokharel & Goldsworthy, 2017; Sapkota et al., 2024).

The 1934 Bihar-Nepal earthquake and the 2015 Gorkha earthquake resulted in extensive destruction, underscoring the seismic risk of the region as well as the vulnerability of the built environment (Bilham, 2019; Gautam & Chaulagain, 2016). Local site effects due to thick lacustrine sediments with depths up to 600 m in places (Paudyal et al., 2012) have played a strong role in determining the severity of impacts of the earthquake in the valley. These soft sediments intensify the ground shaking, generate long period vibrations and may cause soil-structure resonance leading to substantial increase in the likelihood of structural damage and collapse (Dhakal et al., 2012; Pandey et al., 2021).

Although the progress in the seismic risk studies in Nepal has been made in the last decades, most of the studies were performed at regional or macro scales and did not consider the Site-specific variability of the soil response adequately within the Kathmandu Valley (Ranjan et al., 2016). This restriction is a big issue, the site-specific input parameters including the local amplification and resonance effects are still absent in the engineering design codes and urban planning strategies. The fast-growing population, dense infrastructure and cultural heritage of the valley and the lack of detailed seismic microzonation severely hamper disaster risk reduction efforts (Kawase et al., 2011; Pokhrel et al., 2020). The lack of borehole data and the high cost of invasive geotechnical investigation in a densely urbanised environment compounds the problem.

The present study aims to fill this gap through three main objectives: (1) assessing spatial variability of predominant frequency and amplification factor in Kathmandu Valley using Horizontal-to-Vertical Spectral Ratio (HVSR) technique; (2) preparing frequency- and amplification-based seismic microzonation maps classifying soils into very soft, soft and medium categories; and (3) identifying critical areas susceptible to resonance and amplification effects having higher seismic risk. These objectives are framed within the overarching goal of providing data-driven insights to apprise earthquake-resistant designs, urban planning and seismic risk controlling.

The study is based on microtremor data collected from 75 sites, systematically distributed over the Kathmandu, Lalitpur and Bhaktapur districts, in a 500 X 500 m grid. The HVSR method (Nakamura, 1989; Pamuk et al. 2018) was applied due to its low cost, non-invasive nature and applicability in urban areas where intrusive subsurface testing is not feasible and because it has been widely validated in similar sedimentary basins around the world (Lermo & Chávez-García, 1993; Pamuk et al., 2017). The study highlights the predominant frequency and amplification factors to understand the important site response characteristics for microzonation.

The HVSR method primarily provides the fundamental frequency of soft sediments but offers little quantitative constraint on the shear-wave velocity profiles without additional geotechnical data (Konno & Ohmachi, 1998; Bard, 1999). Second, the study area is restricted to the three core districts of the valley and does not include outlying areas, which may also be prone to seismic hazard. Third, the interpretations are based on the ambient vibration records that might not fully capture the non-linear soil behaviour

expected under strong earthquake shaking. The limitations imply that the results are useful for relative zoning and preliminary planning, but in future studies these should be combined with borehole data, geotechnical tests and ground motion data records to improve the data of seismic microzonation of Kathmandu valley.

Significant local diversity in soil response has been noted in previous research (Paudyal et al., 2012; Bijukchhen et al., 2017; Chamlagain & Gautam, 2015). Nevertheless, most assessments depend on sparse measurement networks. Knowledge was advanced by the recent municipal scale microzonation (Sakhakarmi et al., 2024), but it lacked dense coverage throughout the valley and reliable borehole confirmation. This study addresses several research gaps by applying the HVSR method to estimate amplification factors and predominant frequencies at 75 sites distributed on a uniform 500 m $\times$ 500 m grid. Soil conditions are classed into stiff, soft, and very soft categories based on amplification thresholds following SESAME guidelines. Microzonation maps for frequency, amplification, time-period and site classification have been prepared for Kathmandu, Lalitpur and Bhaktapur considering their spatial variation. The study also identifies areas of potential resonance and amplification to help mitigate earthquake risk and aid in urban planning. Finally, this work provides new insights into local seismic site effects, combining borehole-based validation with one of the first valley-wide, high-density HVSR datasets.

Finally, this study fills a major gap in knowledge on seismic microzonation of Kathmandu Valley by generating detailed spatial maps of predominant frequency and amplification using HVSR-based microtremor analysis. The findings strengthen valuable, practical insights for engineers, urban planners and policymakers, thus strengthening the scientific basis for earthquake risk reduction and resilient urban development in one of the world's most seismically vulnerable areas.

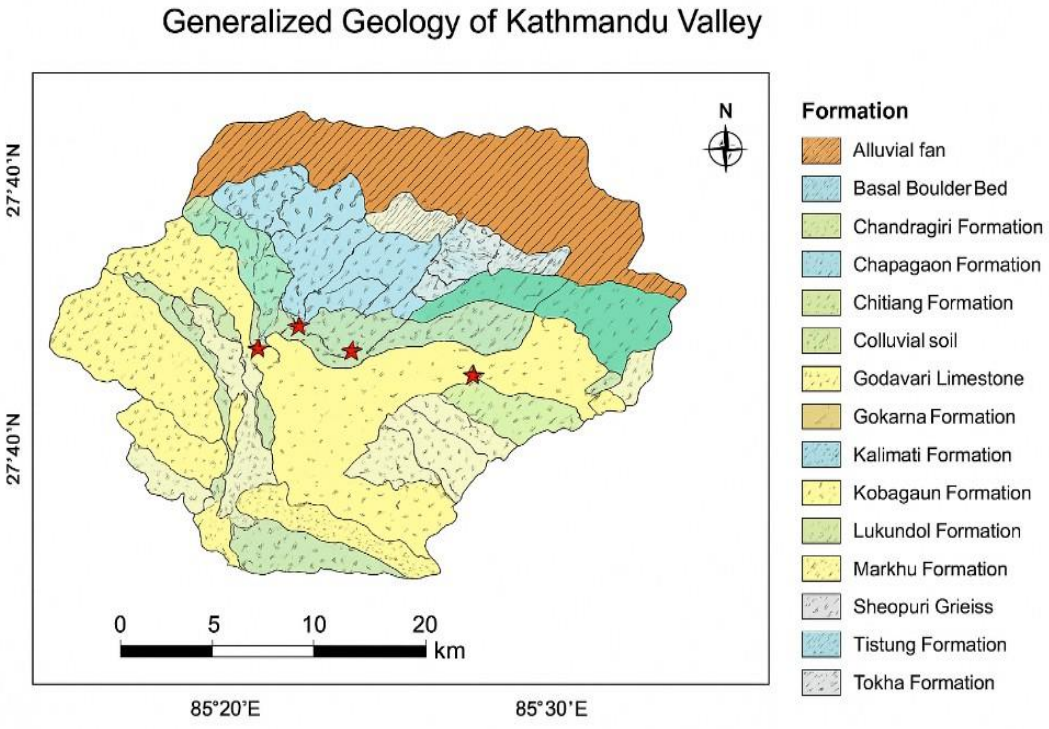


Figure 1. Generalized Geology of Kathmandu Valley Source: (Department of Mines and Geology (DMG), Nepal)

2 Area Of Investigation

The Kathmandu Valley is an intramontane basin in the Lesser Himalayas, characterized by Quaternary lacustrine deposits overlying weathered bedrock (Dangol, 1985). Sediments included clay, silt, sand, and gravel, reaching a thickness of 600 m in the northern-central valley. The surrounding hills are composed of metamorphic and sedimentary rocks, resulting in strong impedance contrasts at the basin margins (Sakai, 2001; Gautam & Yoshida, 1988). The valley is densely built up with medium rise concrete buildings, many of which are susceptible to soil-structure resonance. Figure 1 is the geological engineering map of the Kathmandu Valley and surrounding area prepared by the Department of Mines and Geology (DMG). The research area consists of black clay soil of the Kalimati Formation, recent floodplain deposits of the Hanumante River and basement rocks of the Tistung Formation along the edge of the basin. The fine silt, sand and clay-rich humus that makes up floodplain deposits. Precambrian to Devonian Tistung Formation consists of greenish grey to brown fine-grained phyllite and slate with sand and quartzite. Several studies indicate that Kathmandu Valley is characterised by weak geological formations and very loose soil structures (Chapagain et al. 2010; Kawan et al. 2019). Figure 2 and Figure 3 show the area of investigations and microtremor survey points.



Figure 2. Map Showing Study Area (Kathmandu Valley)

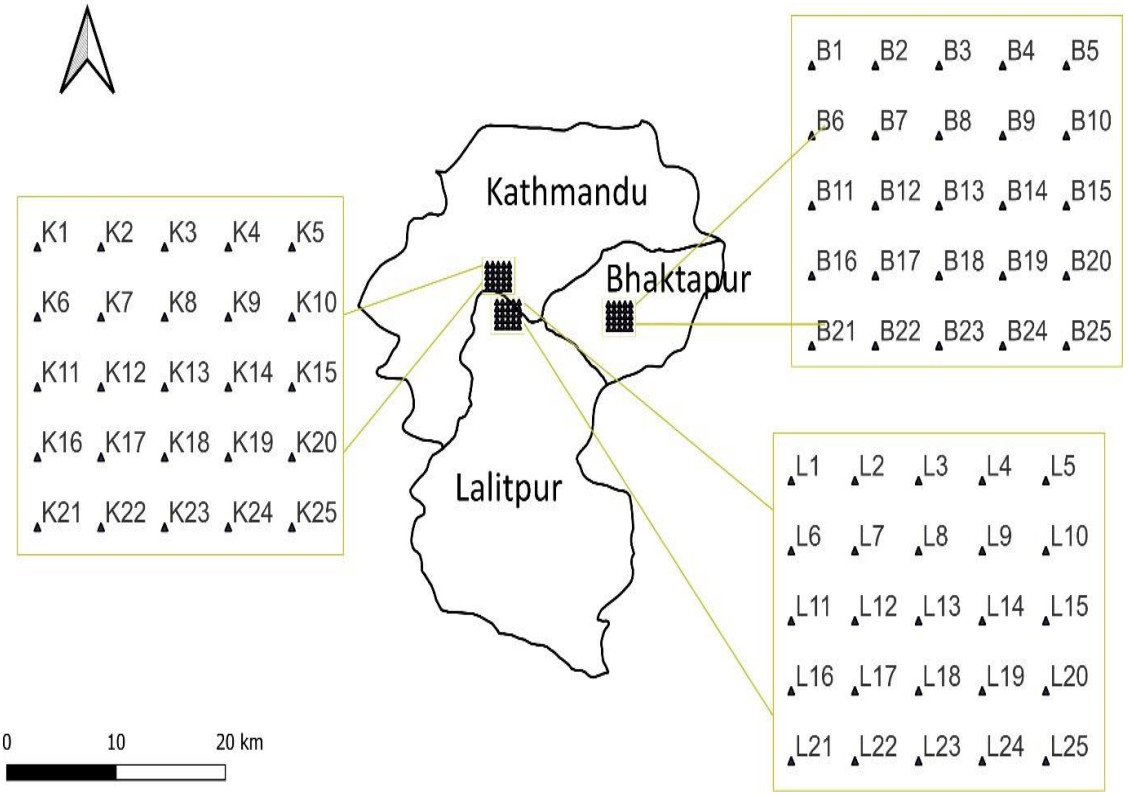
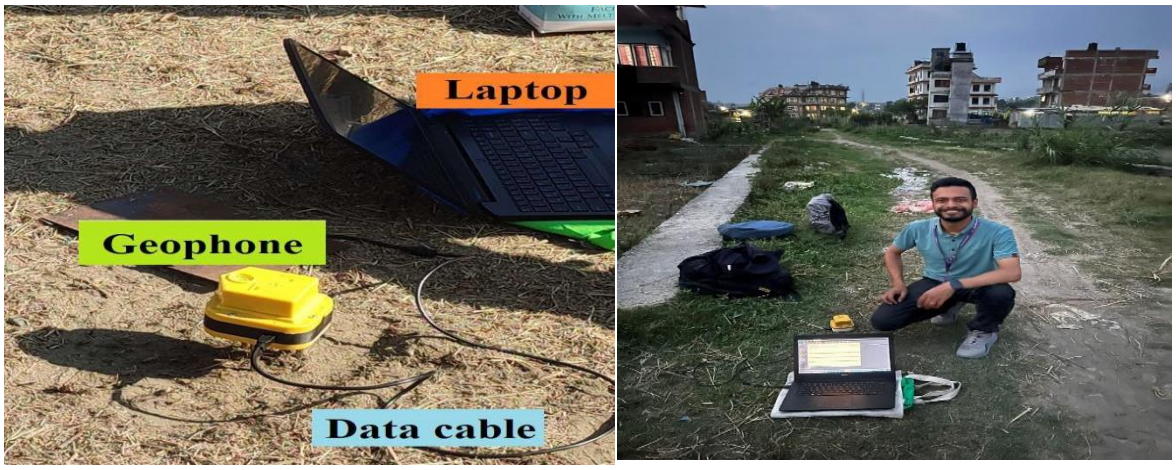


Figure 3. Microtremor Survey points for the Study assigned in Kathmandu Valley (Core area of Kathmandu, Bhaktapur and Lalitpur District Observation Point)

3 Materials And Methodology

3.1 Instrumentation

A portable geophone HG-6, which is small in size, lightweight, and simple to set up, was used for ambient vibration measurements. It is made by HGS (India) Limited, with technology transfer from sensor Nederland BV, and has a natural frequency of 4.5 Hz. Inside the enclosure, the three sensors that comprise the gadget are positioned at right angles to each other the sensor detects three distinct components: one vertical (up-down) direction and two horizontal (east-west and north-south) directions. As illustrated in Figure 4(a) & 4(b), Themino-Dolfrang data-gathering data gathering software (www.theremino.com; Magaro 2016) and a portable laptop were used to capture microtremors in free fields and structures. The HG-6 geophone was utilized in this investigation to gather ambient vibration data because accelerometers are not advised for measuring microtremors because they are insensitive to frequencies lower than 1 Hz (SESAME 2004) and require a long time to set up.



(a) (b)

Figure .4 Microtremor Measurement (a) Instrumentation for the data acquisition and (GPS) of the microtremor station. (b) Instrumental setup for microtremor survey

3.2 Free-field measurements and analysis

Microtremor observations were carried out at 75 strategically distributed sites within Kathmandu, Lalitpur, and Bhaktapur districts. A grid spacing of 500 $\times$ 500 m was used to capture the geological variability within the valley. In total 75 measurement stations, each at 25 stations in the respective Kathmandu, Lalitpur, and Bhaktapur districts, were observed as shown in Fig. 3 above. A Geographic Positioning System (GPS) of the microtremor station. Table 1 displays the configuration of the soil-sensor connection, recording settings, and recording length. At a sampling frequency of 100 Hz, Ambient noise recordings of 30–45 min were collected from each site using portable three-component seismometers. GEOPSY, an open-source program created as part of the SESAME European project, was used to handle and analyze microtremor data. A window length of 20–25 s was used. Stationary windows were selected to provide a minimum of 20 windows for processing and analysis.

The minimum ratio of (STA) to (LTA) was set at 0.2, and the maximum ratio was at 2, to remove transient energy noise (such as footsteps, industrial disturbances, nearby traffic, etc.) from ambient vibration recordings and preserve only quasi-stationary windows (SESAME, 2004). The velocity-time history and noise reduction of all three signal components (N-S, E-W and U-D Directions) are shown in Figure 5. Fast Fourier Transformation (FFT) was then used to analyze each stationary window (each rectangular shape in Figure 5) and produce the Fourier amplitude spectra. The resulting spectra were tapered using a 5% cosine taper after being smoothed with the Konno–Ohmachi smoothing function, with a filter coefficient b value of 40 (Konno and Ohmachi, 1998; Cox et al., 2020). According to Gallipoli et al. (2004), SESAME (2004), Gosar (2010), Gosar et al. (2010), Paudyal et al. (2012), and Molnar et al. (2022), the fundamental frequency of the free field is the frequency corresponding to the distinct HVSR peaks. Because of its ease of comprehension, effectiveness, and computational simplicity, the Inverse Distance Weighted (IDW) method was used for interpolation to create a frequency-based seismic microzonation map (Tuladhar et al., 2004; Paudyal et al., 2012; Wu and Hung, 2016). The processing and analysis of microtremor data were carried out using Python Coding and compared with the results of the Geopsy. The measurements must be taken at mid-

night, when social activities almost end, in order to eliminate the impact of a tremor whose source can be identified. However, this process substantially lessens the benefits of the microtremor "Nakamura" method. The (HVSR) methodology is one of the most widely used methods for assessing ground responses using microtremor readings. Using microtremor recordings, this approach measures the ground motion spectra in both horizontal and vertical directions. The data was processed according to SESAME (2004) guidelines. Noise-free time windows were selected, and Fourier spectra were computed. The Horizontal-to-Vertical Spectral Ratio (HVSR) method was applied to extract the predominant frequency (Fp) corresponding to the HVSR peak and amplification factor (Ap) corresponding to its amplitude.

According to Nakamura (1989),the HVSR is given by:

$$\mathrm{HVSR}(\omega) = \frac{\sqrt{F_{NS,i}^2(\omega) + F_{EW,i}^2(\omega)}}{F_{UD,i}(\omega)} \quad (1)$$

Where,

FNSi(w)2 and FEWi(w)2 are north-south and east-west Fourier amplitudes, respectively. Each interval's up-and-down components, with w being the frequency.

The HVSR curve provides valuable information regarding the soil properties of the site and its susceptibility to local soil amplification. Several key observations can be made. The fundamental frequency of the soil column is frequently associated with the frequency at which the HVSR curve reaches its highest value. This frequency can give insights about the depth of the groundwater table and the soil layering and stratification at the site. The amplitude of the HVSR peak can indicate the site's potential for amplifying ground motions, which can be relevant for assessing the potential for liquefaction.

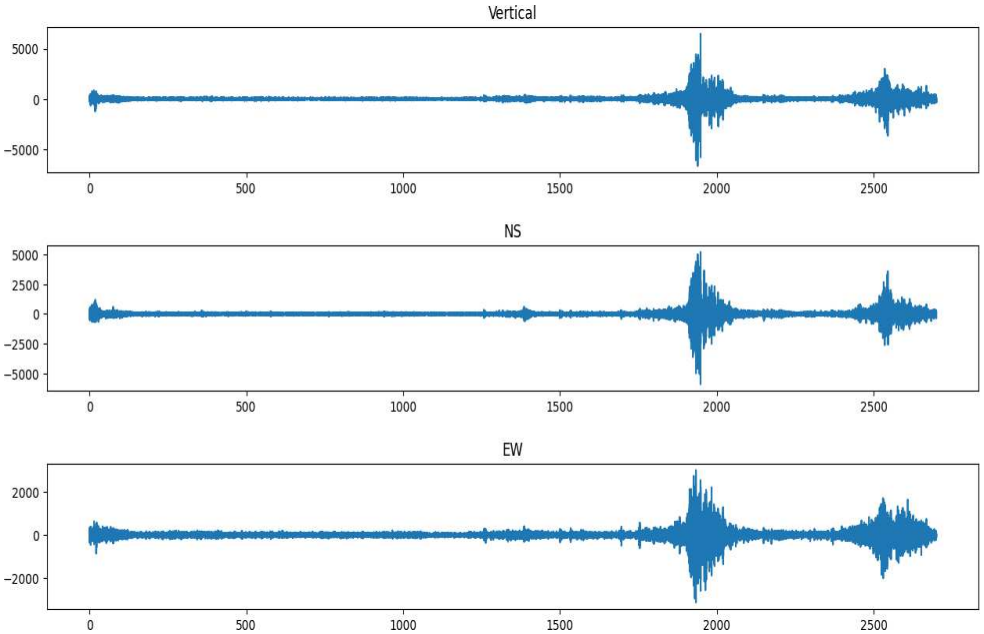


Figure 5. Typical microtremor data measurement pattern with N-S, E-W and U-D Directions

3.3 Calculation of Natural Period of Layered soil

Sum of layer periods: According to Sawada(2004),the natural period was found to be a twice-two-way period by summing the times that a shear wave travels through each stratum.

$$T_c = 4 \sum_{i=1}^{N} \frac{H_i}{V_i}, \tag{2}$$

where, as seen in figure 6 (Sawada, 2004), Tc refers to Characteristic Period of the soil profile, Vi and Hi stand for the ith layer's thickness and shear velocity and N refers Number of Layers (excluding bedrock).

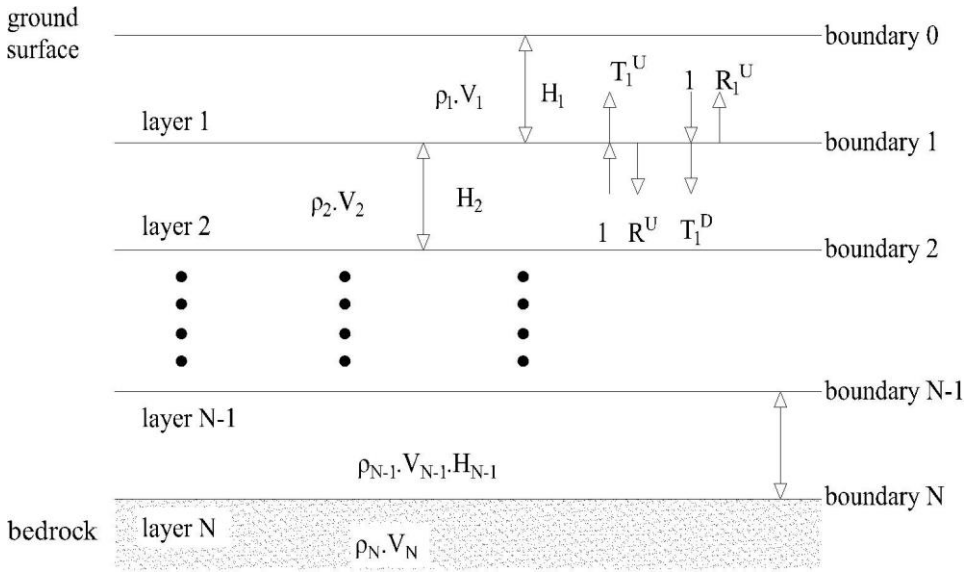


Figure 6. Parameters of ground model (Sawada, 2004)

3.4 Soil Classification and Mapping

Sites were categorized into three soil classes according to the SESAME Guidelines based on Ap values: Ap < 2 (stiff soil or rock),2 ≤ *Ap* < 4_*softsoil*), *and*Ap ≥ 4 (very soft or deep soft sediments). Spatial interpolation was applied to develop preliminary microzonation maps for Fp, Ap, time-period, and Soil Classification.

3.5 Seismic Zoning Types

Stable zones are characterized by a lower amplification factor (Amp < 1) and, a higher frequency (shorter time-period, usually <0.5 s), and typically may indicate corresponding to stiffer or soft soil (not "very soft"). Similarly, areas susceptible to local amplification exhibit moderate frequencies (1–2 Hz) with amplification > 2, and even in cases where the soil is " soft," these locations exhibit considerable amplification and intense shaking during seismic activity. Finally, the most dangerous zones are those that are prone to instability (resonance, liquefaction potential, ground failure), with very low frequencies (<1.5 Hz, time-period > 0.7–0.8 s), high amplification (>3), and soil classification may indicate very soft.

3.6 Analytical Evaluation

Ground acceleration as a function of time is displayed in the time-history record. The beginning of the record is somewhat modest, followed by a strong-motion interval that lasts from 10 to 40 seconds, after which there is a slow decrease with ongoing oscillations. The rebuilt series shows a peak absolute acceleration of roughly 0.165 *g*, which is in line with the earthquake input motion discussed in the manuscript. Because it maintains the input motion's duration and amplitude properties, this record is crucial for site-response analysis. Because it has the most cycles, the strong-motion section makes the biggest contribution to the computed soil response. The input motion is propagated across the soil profile for DEEPSOIL analysis in order to assess how local ground conditions alter the amplitude and frequency content.

3.7 Conceptual Basis of One-Dimensional Site-Response Modeling

The soil deposit is idealized as a stack of horizontal layers overlying a relatively rigid bedrock. For vertically propagating SH waves, the seismic response can be represented by the one-dimensional shear-wave equation. Let $u(z, t)$ denote horizontal particle displacement, $\rho(z)$ the mass density, and $G(z)$ the shear modulus. According to Kramer (1996), the governing equation is

$$\frac{\partial}{\partial z}\left[G(z)\frac{\partial u(z,t)}{\partial z}\right] = \rho(z)\frac{\partial^2 u(z,t)}{\partial t^2}. \tag{1}$$

Kramer (1996) explained for a homogeneous layer in which G and ρ are constant, the governing equation reduces to the classical wave equation:

$$\frac{\partial^2 u}{\partial z^2} = \frac{1}{V_s^2}\frac{\partial^2 u}{\partial t^2}. \tag{2}$$

The shear-wave velocity is related to shear modulus and density given by Kramer (1996),

$$V_s = \sqrt{\frac{G}{\rho}}. \tag{3}$$

Therefore, the stiffness of each soil layer can be represented either by G or by V_s. The supplied manuscript states that V_s was used to define soil stiffness in the present analysis.

3.8 Layered-Soil Transfer Function

For harmonic SH-wave motion, displacement in a homogeneous layer can be expressed as the superposition of upward- and downward-propagating waves by Kramer (1996):

$$u(z, t) = \left[Ae^{-ikz} + Be^{ikz}\right]e^{i\omega t}. \tag{4}$$

where A and B are wave amplitudes, ω is circular frequency, and k is the wave number:

$$k = \frac{\omega}{V_s} = \frac{2\pi f}{V_s}. \tag{5}$$

The shear stress associated with the wave given by Kramer (1996) is

$$\tau(z,t) = G\frac{\partial u}{\partial z}. \tag{6}$$

At an interface between two layers, displacement and shear-stress continuity are imposed:

$$u_1 = u_2, \tag{7a}$$

$$\tau_1 = \tau_2. \tag{7b}$$

These boundary conditions account for impedance contrasts between adjacent layers. The seismic impedance of a layer given by Kramer (1996) is

$$Z = \rho V_s. \tag{8}$$

A large impedance contrast between soft sediment and stiff underlying material can generate substantial wave reflection and constructive interference. The frequency-dependent surface response can therefore be expressed through a transfer function provided by Kramer (1996):

$$H(f) = \frac{A_{\text{surface}}(f)}{A_{\text{bedrock}}(f)}. \tag{9}$$

where $A_{\text{surface}}(f)$ and $A_{\text{bedrock}}(f)$ are the Fourier amplitudes at the ground surface and engineering bedrock, respectively. The amplification factor at a particular frequency may consequently be written as

$$AF(f) = |H(f)|. \tag{10}$$

3.9 Fundamental Frequency and Resonance of the Soil Column

For a simplified homogeneous soil layer of thickness H over rigid bedrock, the fundamental resonance frequency is approximately governed by the quarter-wavelength relation explained by Kramer (1996):

$$f_0 \approx \frac{V_s}{4H}. \tag{11}$$

According to Kramer (1996),for a multilayer soil column, a more appropriate interpretation is obtained by considering the travel time through all layers:

$$f_0 \approx \frac{1}{4\sum_{i=1}^{n} \frac{h_i}{V_{s_i}}}. \tag{12}$$

where h_i and V_{s_i} are the thickness and shear-wave velocity of layer i. This formulation is particularly useful for interpreting the observed HVSR fundamental frequency against the borehole/MASW/DEEPSOIL model. A low fundamental frequency generally indicates a relatively thick and/or soft sedimentary column, whereas a higher frequency is generally associated with thinner and/or stiffer material.

3.10 Estimation of Shear-Wave Velocity from SPT-*N* Values

The supplied manuscript uses an empirical SPT-*N* to shear-wave velocity relationship for defining the stiffness profile:

$$V_s = 97N^{0.314}. \tag{13}$$

where V_s is in m/s and N is the SPT blow count. This relationship is explicitly reported in the supplied manuscript and is attributed there to Ordóñez (2006). For each soil layer, the estimated V_s can be used to calculate the maximum shear modulus by Kramer (1996):

$$G_{\max} = \rho V_s^2. \tag{14}$$

The manuscript also cites Kathmandu Valley-specific correlations reported by Gautam (2017), including

$$V_s = 115.8N^{0.251}, \quad \text{all soils,} \tag{15a}$$

$$V_s = 102.4N^{0.247}, \quad \text{silt,} \tag{15b}$$

$$V_s = 78.7N^{0.352}, \quad \text{sand.} \tag{15c}$$

For the final PhD manuscript, the selected V_s–N relationship should be justified according to soil type, calibration dataset, and applicability to Kathmandu Valley. If the Ordóñez relationship is retained for the main model, the Kathmandu-specific correlations can be presented as an independent sensitivity or validation comparison rather than mixing correlations within one profile.

3.11 V_{s30} Calculation and Engineering Site Classification

The average shear-wave velocity of the upper 30 m is calculated using the travel-time weighted expression by Kramer (1996):

$$V_{s30} = \frac{30}{\sum_{i=1}^{} \frac{h_i}{V_{s_i}}}. \tag{16}$$

where h_i is the thickness of each layer within the upper 30 m, and V_{s_i} is its shear-wave velocity. V_{s30} is important because it provides a standardized indicator of near-surface stiffness and is used by several seismic site-classification frameworks. The supplied manuscript notes that the upper 30 m is a fundamental factor influencing ground motion and discusses V_{s30} in connection with NEHRP/IBC site classification.

3.12 Equivalent-Linear Formulation

In equivalent-linear site-response analysis, the nonlinear behavior of soil is represented by strain-compatible effective shear modulus and damping. According to Kramer (1996),the modulus reduction ratio is

$$\frac{G}{G_{\max}} = \frac{G(\gamma)}{G_{\max}}. \tag{17}$$

where γ is the representative shear strain. The equivalent damping ratio can be denoted by

$$\xi_{eq} = \xi_{eq}(\gamma). \tag{18}$$

The analysis is performed iteratively. A typical iteration sequence is:

[label=(xii)]

1. assign initial G_{max} and damping;
2. calculate the strain response;
3. determine effective strain;
4. update G/G_{max} and damping using the selected soil curves; and
5. repeat until the change in strain-compatible properties satisfies the convergence criterion.

The supplied manuscript identifies DEEPSOIL as the software used for one-dimensional equivalent-linear frequency-domain analysis, including convolution and deconvolution.

3.13 Nonlinear Time-Domain Formulation

Kramer (1996), explained for nonlinear analysis, the soil response can be formulated through the equation of motion in the time domain:

$$\rho(z)\frac{\partial^2 u}{\partial t^2} = \frac{\partial \tau}{\partial z}. \tag{19}$$

with a nonlinear constitutive relationship

$$\tau = \tau\left(\gamma, \dot{\gamma}, \text{history}\right). \tag{20}$$

where γ is shear strain, $\dot{\gamma}$ is strain rate, and the response may depend on loading history. The tangent shear modulus is

$$G_{tan} = \frac{\partial \tau}{\partial \gamma}. \tag{21}$$

The nonlinear formulation allows stiffness and damping characteristics to evolve with strain during the earthquake motion. This provides a physical explanation for why nonlinear amplification may be lower than equivalent-linear amplification at large strains in some parts of the valley.

3.14 Fourier Analysis of the Earthquake Input Motion

For an acceleration time history $a(t)$, the Fourier transform is defined by Kramer (1996) as

$$A(f) = \int_{-\infty}^{\infty} a(t) e^{-i2\pi ft}\, dt. \tag{22}$$

The Fourier amplitude spectrum is

$$FAS(f) = |A(f)| . \tag{23}$$

The FAS identifies the frequency content of the Gorkha earthquake input motion. Comparing the dominant frequencies of the input motion with the soil fundamental frequency provides a first-order assessment of the potential for resonance.

3.15 Response-Spectrum Formulation

For a single-degree-of-freedom oscillator with natural circular frequency ω_n and damping ratio ξ, the relative displacement response to ground acceleration $a_g(t)$ is governed by

$$\ddot{u} + 2\xi\omega_n\dot{u} + \omega^2 u = -a_g(t). \tag{24}$$

The spectral acceleration is then obtained from the maximum absolute relative displacement:

$$S_a(T, \xi) = \omega_n^2 \max_t |u(t)| . \tag{25}$$

where

$$T = \frac{2\pi}{\omega_n}$$

is the natural period. Response spectra from the input and surface motions can therefore be compared to quantify the modification of earthquake demand by the soil profile.

3.16 Amplification Factor and Spectral Amplification

A simple time-domain amplification ratio may be defined as

$$AF_{PGA} = \frac{PGA_{\text{surface}}}{PGA_{\text{bedrock}}}. \tag{26}$$

For frequency-domain analysis, spectral amplification at frequency f can be expressed as

$$AF(f) = \frac{|A_{\text{surface}}(f)|}{|A_{\text{bedrock}}(f)|}. \tag{27}$$

Similarly, period-dependent response-spectrum amplification may be expressed as

$$AF(T) = \frac{S_{a,\text{surface}}(T)}{S_{a,\text{bedrock}}(T)}. \tag{28}$$

These definitions should not be interchanged without stating whether the reported amplification is based on PGA, Fourier amplitude, or response-spectrum acceleration. This distinction is important when comparing the amplification maps in Figures 43 and 44 with HVSR amplification values.

3.17 HVSR Theoretical Formulation

For three-component ambient-noise measurements,Nakamura (1989) defined the horizontal-to-vertical spectral ratio can be represented by

$$HVSR(f) = \frac{H(f)}{V(f)}. \tag{29}$$

where a common formulation of the horizontal component is the geometric mean of the two horizontal components:

$$H(f) = \sqrt{NS(f)\,EW(f).} \tag{30}$$

Therefore,

$$HVSR(f) = \frac{\sqrt{NS(f)\,EW(f)}}{V(f)}. \tag{31}$$

The frequency at which a stable, physically meaningful HVSR peak occurs is interpreted as the fundamental site frequency f_0, provided that the peak satisfies the adopted quality-control criteria. The theoretical site-response frequency from the soil column can then be compared with the measured HVSR frequency.

3.18 Mathematical Comparison Between Observed and Modeled Frequency

For validation, the difference between the measured microtremor frequency and the modeled/borehole frequency can be quantified using absolute and percentage error:

$$e_i = \left| f_{0,\text{measured}} - f_{0,\text{modeled}} \right|. \tag{32}$$

$$PE_i = \frac{\left| f_{0,\text{measured}} - f_{0,\text{modeled}} \right|}{f_{0,\text{modeled}}} \times 100. \tag{33}$$

For N validation stations,Willmott & Matsuura (2005) defined the mean absolute error is

$$MAE = \frac{1}{N} \sum_{i=1}^{N} \left| f_{0,\text{measured},i} - f_{0,\text{modeled},i} \right|. \tag{34}$$

and the root-mean-square error is

$$RMSE = \sqrt{\frac{1}{N} \sum_{i=1}^{N} \left(f_{0,\text{measured},i} - f_{0,\text{modeled},i} \right)^2}. \tag{35}$$

These statistics can be extended to V_{s30} or amplification-factor validation. Lower RMSE indicates closer agreement between the modeled and measured quantities, although model quality should also be assessed using physical plausibility and spatial consistency rather than a single error metric.

3.19 Mathematical Basis for Spatial Microzonation

Shepard (1968) explained for spatial prediction of a parameter Z at an unsampled location, inverse-distance weighting (IDW) can be written as

$$\hat{Z}(x_0) = \frac{\sum_{i=1}^{n} w_i Z(x_i)}{\sum_{i=1}^{n} w_i}. \tag{36}$$

where

$$w_i = \frac{1}{d_i^p}. \tag{37}$$

Here, d_i is the distance between the prediction location and observation i, and p is the distance-decay power. The IDW surface is therefore controlled strongly by nearby observations.

According to Cressie (1993),if Kriging is also evaluated, the ordinary-Kriging estimator can be represented as

$$\hat{Z}(x_0) = \sum_{i=1}^{n} \lambda_i Z(x_i), \tag{38}$$

subject to

$$\sum_{i=1}^{n} \lambda_i = 1. \tag{39}$$

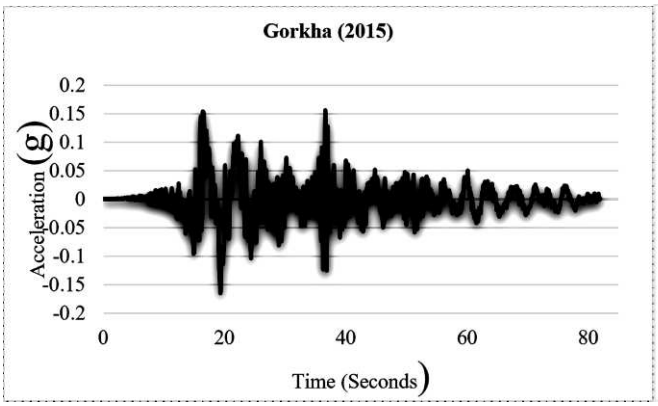
The Kriging weights λ_i are obtained from the spatial covariance or semivariogram structure. For model selection, cross-validation can compare RMSE, MAE, bias, and residual spatial patterns. The interpolation method should be selected based on both statistical performance and geological/seismological plausibility.

When a fault ruptures below the earth's surface, body waves travel away from the source in all direction. As they reach boundaries between different geologic materials, they are reflected and refracted . since the wave propagation velocities of shallower materials are generally lower than the materials beneath them, inclined rays that strikes horizontal layer boundaries are usually reflected to a more vertical direction. By the time the rays search the ground surface, multiple refraction has often bent them to a nearly vertical direction. One-dimensional ground response analyses are based on the assumption that all boundaries are horizontal and that the response of a soil deposit is predominately caused by shear wave propagating from underlying bedrock. For one-dimensional ground response analysis, the soil and bedrock surfaces are assumed to extend infinitely in the horizontal direction. Procedure based on this assumption have been shown to predict ground response that is in reasonable agreement with measured response in many cases. Deepsoil is a one-dimensional site response analysis program that can perform 1-D equivalent linear frequency domain analyses including convolution and deconvolution. The stiffness of soil can be defined either by defining the shear modulus value or by defining the shear wave velocity value of the deposit. In present analysis, shear wave velocity has been considered for defining stiffness of soil. So, for evaluating shear-wave velocity

(Vs) profiles, the SPT-N values are used through available correlations. The relation, $V_s = 97N^{0.314}$, is applicable for all type of soils is used in the analysis, where Vs is in m/s (Ordóñez, 2006). Rigid bedrock is used in the analysis and the rigidity for elastic bedrock is obtained by considering a very high shear wave velocity ($\approx$ 5*107m/sec) (Kumar et al., 2014). the input motions considered for present analysis is the most recent Nepal earthquake of magnitude Mw=7.8. Peak Ground Acceleration (PGA) Mw=7.8 earthquake is observed as 0.162g at 49.34sec as per the earthquake time histories.

1D ground response analysis is the technique use to analyse the three-dimensional nonlinear soil deposits. 1D ground response analysis mainly follows any of the three methods such as; linear, However, nonlinear method uses direct numerical integration in the time domain to analyse the actual nonlinear response of the soil deposit. Integration in small time steps allow to use the appropriate soil properties in that time step. In the paper by M.R. pandey: microzoning of Kathmandu Valley based on soil amplification, Nepal seismological laboratory, Department of Mines and Geology, 1986, the microtermor data of different sites of Kathmandu valley canbe used to access site response and amplification factor due to unconsolidated sediments. This allows microzoning on the basis of soil amplification of results of micrometer are correlated with distribution of facies of unconsolidated sediments in the valley, the maximum amplitude of micrometor being observed in the central area where a 200-350m lacustrine clayey sediments overlies a 200-250m thick sandy fluviatile section. Theoretical response of vibrational built up of S-waves due to multiple reflections predict relative amplification by a factor of 5 to 6 in the central part of the valley in comparison to bed rock and northern part of reasonable S-wave impedance contrast. Estimate of relative amplification from observed maximum peak power amplitude in the high amplitude area, however does not exceed the predicted relative amplification by more than a factor of 2.

Dipendra Gautam (2017) Empirical correlation between uncorrected standard penetration resistance (N) and shear wave velocity (VS) for Kathmandu Valley, Nepal Vs,30=ANB power equation model NEHRP and IBC accept VS,30 as the fundamental input parameters and representative indicator and Kiku et al. (2001) stated that the upper 30 m of soil stratum is the fundamental factor influencing the ground motions For all soils $V_s = 115.8N^{0.251}$ (R2=0.623)For silt; $V_s = 102.4N^{0.247}$ (R2=0.355);For Sand $V_s = 78.7N^{0.352}$ (R2=0.441).



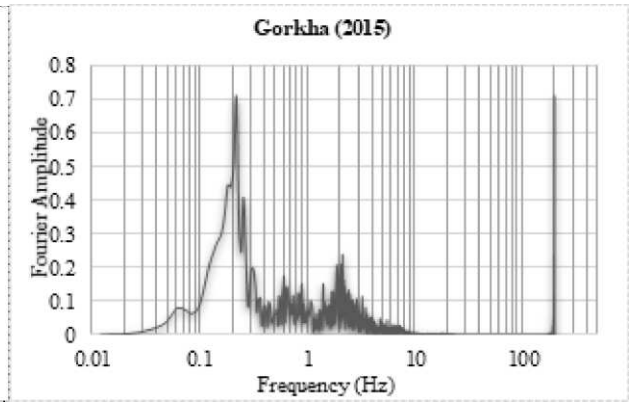


Fig. 7. Gorkha Earthquake (2015) Time History Plot *Fig. 8. Fourier Amplitude Spectrum for Gorkha Earthquake*

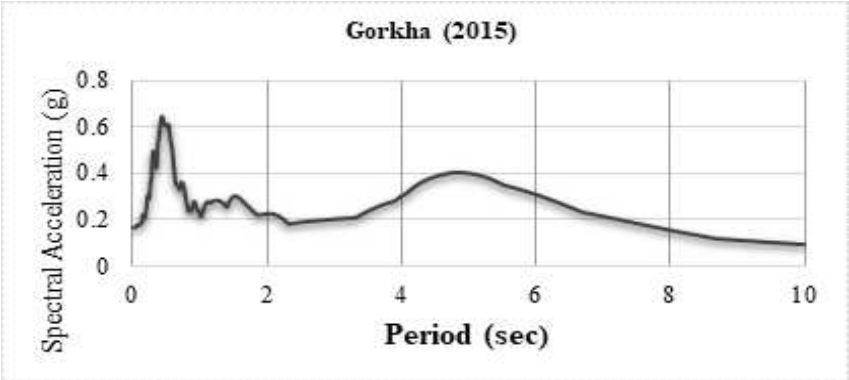


Fig. 9. Response Spectrum for Gorkha Earthquake

4 Results And Discussions

4.1 Free-Field Site Characteristics in Central Bhaktapur

As shown in figure 6 and 7, the instrument survey findings are expressed in terms of the predominant frequency and amplification factor in the stations. As observed in the above Figure 8, Figure 9, Figure 10 and Figure 11, microtremor observation points predominant frequency ranges from 0.44Hz to 5.123Hz likewise, Amplitude ranges from 1.003 to 4.39. Figure 4: Typical E-W, N-S, U-D respective directions of recorded microtremor data. Station B-1, B-2, B-5, B-13, B-17, B-18, B-20, B-22, B-23 soil was found to be soft soil whereas Station B21 is classified to very soft soil other remaining stations are found stiff soils.

Station B-23, Station B-9 demonstrates that the samples of the HVSR graph with frequency that represents the thick sediment deposits over the basement rock could result in the site's low frequency. Significantly higher frequencies with distinct HVSR curves (station B-12, Figure 9; station B-13, Figure 10) are constituted by the basin's edges and some parts of the center region in the study area, which might be an indication of shallow sediment deposits over the underlying bedrock.

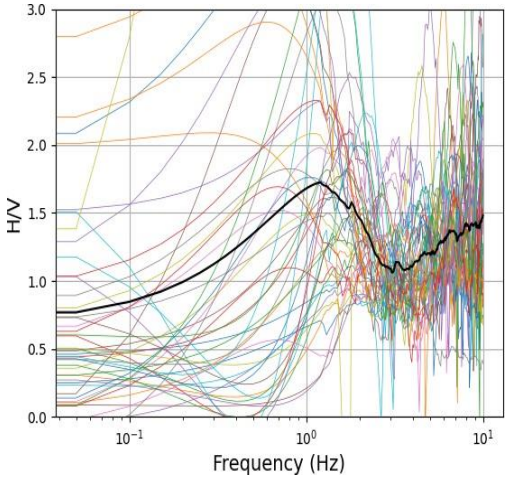


Figure 10.HVSR Plot of Station B4

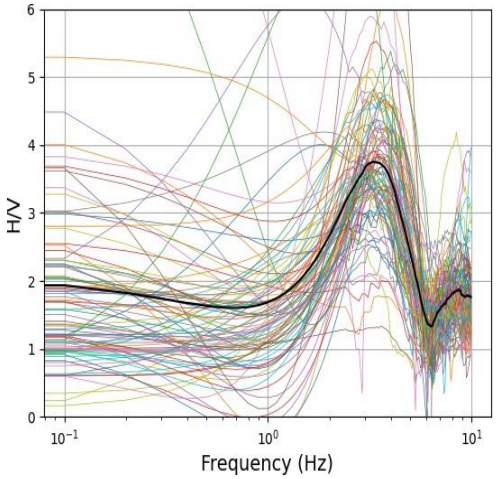


Figure 11. HVSR Plot of Station B21

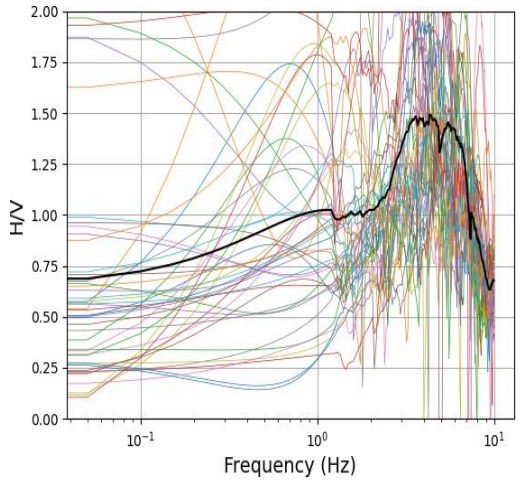


Figure 12. HVSR Plot of Station B12

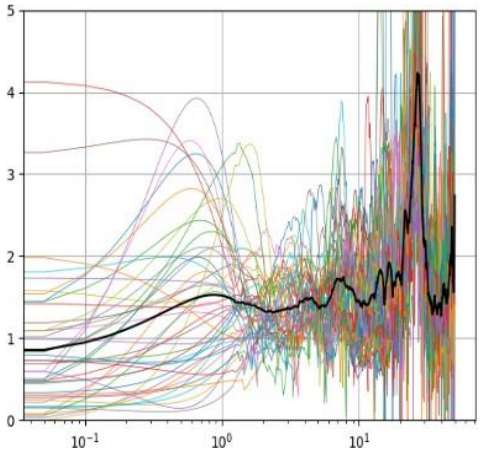


Figure 13. HVSR Plot of Station B13

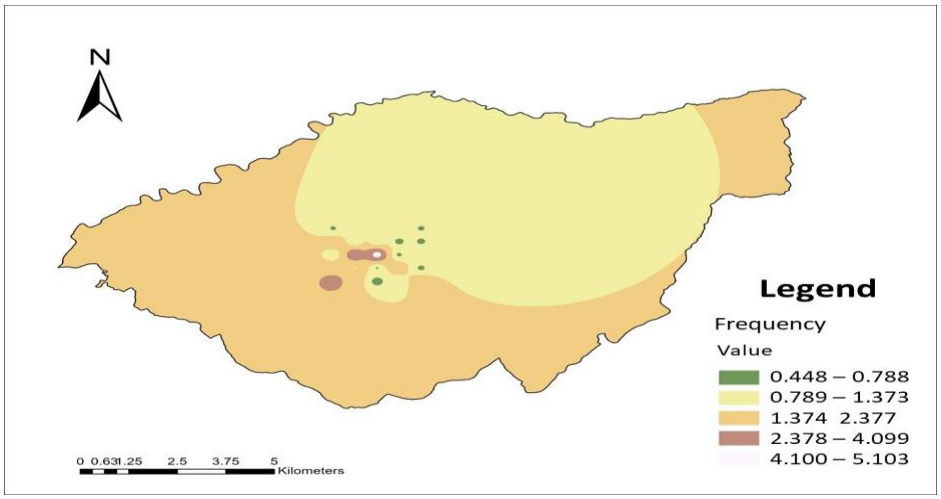


Figure 14. Predominant frequency zoning of core area of Bhaktapur district

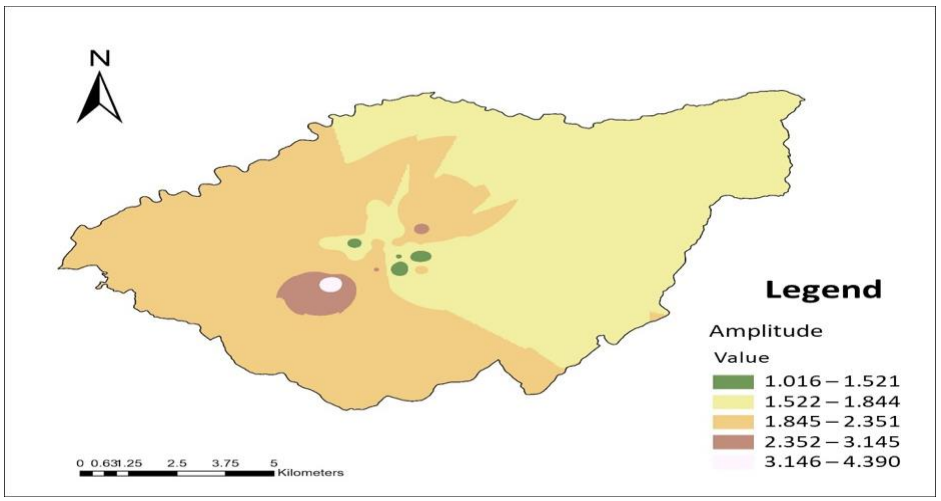
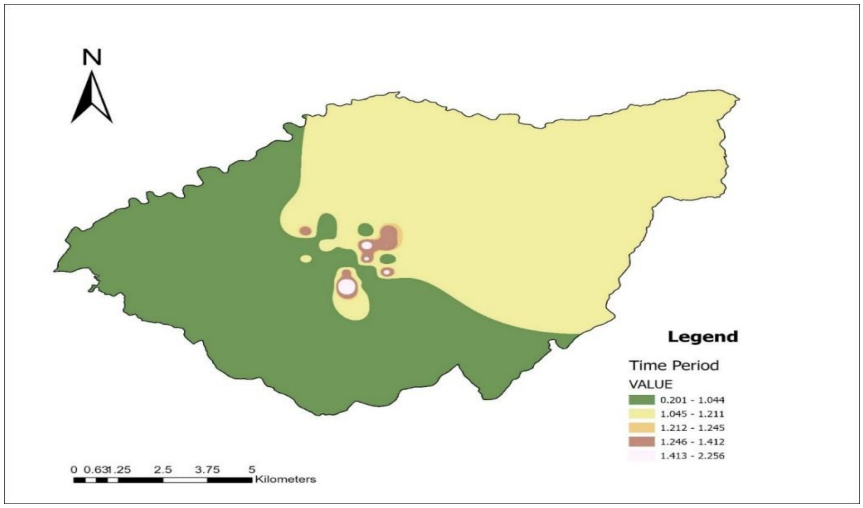


Figure 15. Amplification factor zoning of core area of Bhaktapur district

708 Table 1. Predominant frequency, Amplification factor, Time period and HVSR based
709 site class of Bhaktapur Stations
710

Station	Latitude	Longitude	Amplitude	Frequency (Hz)	Time period (Sec)	HVSR-based site class
B-1	27.681027	85.417986	2.201	0.720	1.389	Soft soil
B-2	27.681027	85.423065	2.221	1.207	0.829	Soft soil
B-3	27.681027	85.428143	1.530	0.850	1.176	Stiff soil
B-4	27.681027	85.433221	1.736	1.178	0.849	Stiff soil
B-5	27.681027	85.438300	2.680	0.748	1.337	Soft soil
B-6	27.67653	85.417987	1.528	1.722	0.581	Stiff soil
B-7	27.67653	85.423065	1.182	0.826	1.211	Stiff soil
B-8	27.67653	85.428143	1.922	0.899	1.112	Stiff soil
B-9	27.67653	85.433221	1.905	0.615	1.626	Stiff soil
B-10	27.67653	85.438299	1.853	0.705	1.418	Stiff soil
B-11	27.672032	85.417987	2.043	0.877	1.140	Stiff soil
B-12	27.672033	85.423065	1.69	3.90	1.009	Stiff soil
B-13	27.6720328	85.4281432	2.087	5.123	0.195	Soft soil
B-14	27.672033	85.433221	1.489	0.678	1.475	Stiff soil
B-15	27.672032	85.438299	1.139	1.178	0.849	Stiff soil
B-16	27.667536	85.417987	1.877	1.371	0.729	Stiff soil
B-17	27.667536	85.423065	2.006	1.350	0.741	Soft Soil
B-18	27.667536	85.428143	2.420	0.730	1.370	Soft Soil
B-19	27.667536	85.433221	1.003	1.795	0.557	Stiff soil
B-20	27.667536	85.438299	2.000	0.670	1.493	Soft Soil
B-21	27.663038	85.417988	4.394	3.592	0.278	Very soft
B-22	27.663038	85.423065	2.351	1.561	0.641	Soft Soil
B-23	27.663038	85.428143	2.165	0.442	2.262	Soft Soil
B-24	27.663038	85.433221	1.620	1.043	0.959	Stiff soil
B-25	27.663038	85.438298	1.688	1.946	0.514	Stiff soil

711 (Soil Classification Based on Amplification (SESAME,2004))
712



713 *Figure 16. Time period zoning of core area of Bhaktapur district*

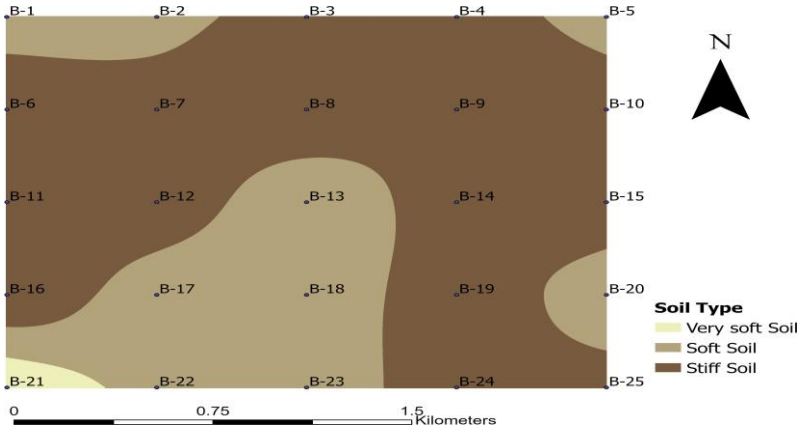


Figure 17. HVSR based site class zoning of core area of Bhaktapur district

Table 1 shows the location with predominant frequency, amplification factor, time-period, and HVSR based site class of Bhaktapur stations. Fig. 11,12,13 and 14 are zonation maps on a scale of 1:5,000 scale in terms of frequency, amplification, time-period, and HVSR based site class classifications of the Bhaktapur district. Our HVSR analysis zoning obtained for Bhaktapur for B-21 and B-13 show short periods (stiffer layers) but very high amplification classic local site amplification risk. B-1, B-5, B-18, and B-23 combine long periods with amp ≥ 2*suggestspotentialforinstability/resonanceinverysoftdeposits, andB*−19*isastablesite*.

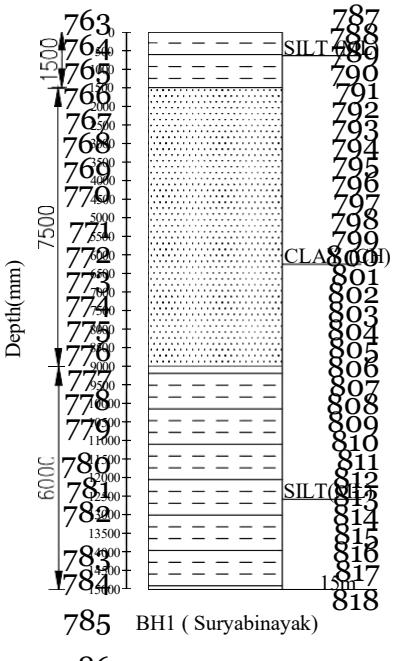


Figure 18. Bore hole BH1-Suryabinayak, core area of Bhaktapur district

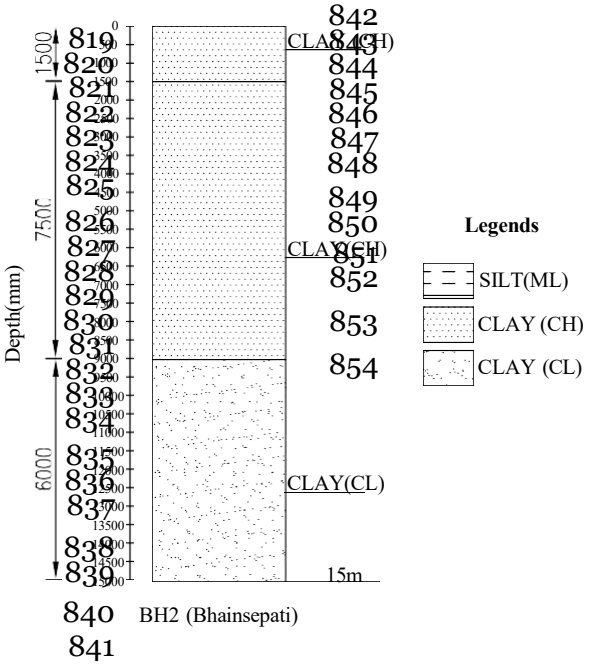


Figure 19. Bore hole BH2-Bhainsepati, core area of Lalitpur district

One borehole log data point was considered, as illustrated in Figure 15 BH-1 in Suryabinayak near B-21, to validate the results. This verification shows that rocky sites

or very thin sediment deposits are associated with high fundamental frequency, while thick sediment deposits (D'Amico et al. 2004; Birgoren et al. 2009; Paudyal et al. 2012). The lithological features of the borehole were categorized based on the Unified Soil Classification System (USCS) adopted by ASTM (1996), as shown in Figure 15. BH1 lies in the southern part (near station B21) and comprises of shallow sediment deposits over the bedrock.

4.2 Free-Field Site Characteristics in Central Lalitpur

The Predominant frequency of the microtremor observation points ranged from 0.553HZ to 5.448Hz and the amplitude ranged from 1.027 to 3.642. Station L-3, L-7(Figure 17), L-13, L-14, L-21 soil was found to be soft soil whereas other remaining stations are found stiff soils. Stations L13 and station L17, (Figure 19) demonstrate that the samples of the HVSR graph with frequency, which represent the thick sediment deposits over the basement rock, could result in the site's low frequency. Significantly higher frequencies with distinct HVSR curves (station L24, Figure 20) are constituted by the basin's edges and some parts of the central region in the study area, which might be an indication of shallow sediment deposits over the underlying bedrock. One borehole log data point was considered, as illustrated in Figure 20, to validate the results. This verification shows that rocky sites or very thin sediment deposits are associated with high fundamental frequency, while thick sediment deposits (D'Amicoet al. 2004; Birgoren et al. 2009; Paudyal et al. 2012). The lithological features of the borehole were classified based on the Unified Soil Classification System (USCS) adopted by ASTM (1996), as shown in Figure 16. BH2 lies in the southern part (near station L-24) and comprises of shallow sediment deposits over the bedrock.

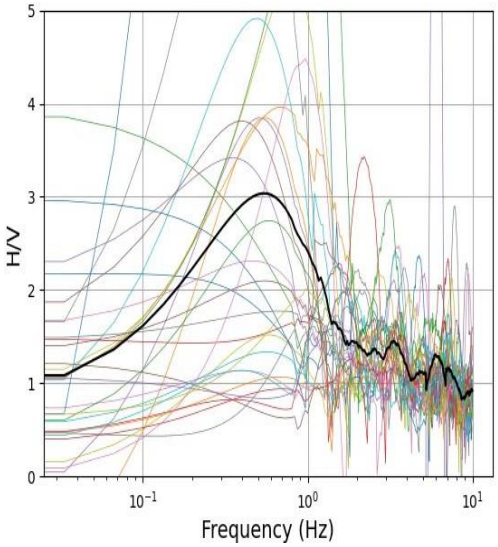


Figure 20. HVSR Plot of Station L7

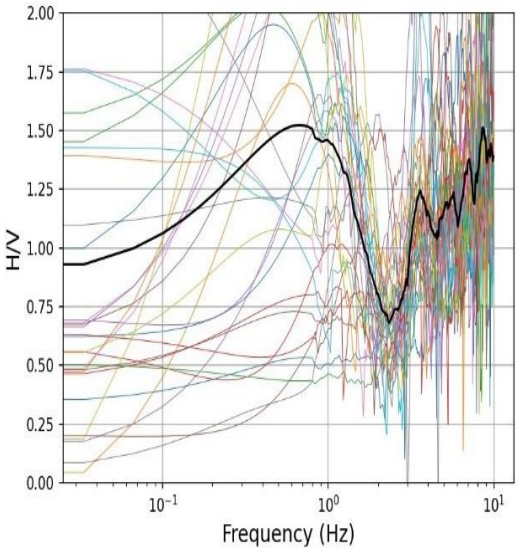


Figure 21. HVSR Plot of Station L19

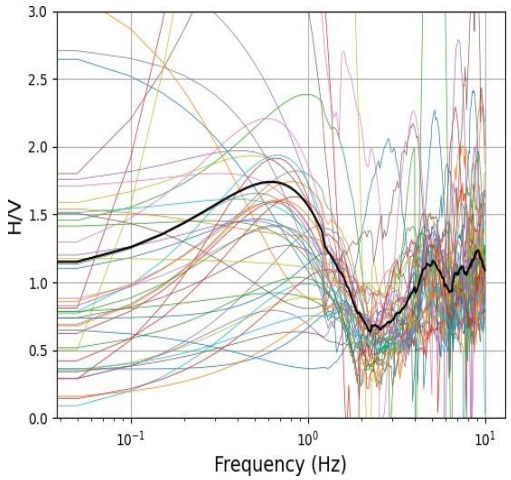


Figure 22. HVSR Plot of Station L17

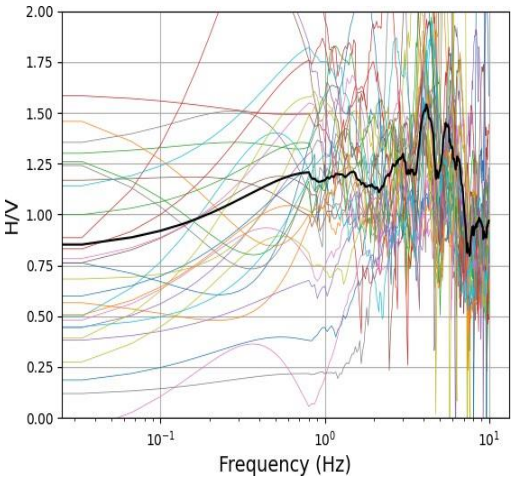


Figure 23. HVSR Plot of Station L24

Figure 21, Figure 22, Figure 23 and Figure 24 are zonation maps on scale of 1:5000 in terms of frequency, amplification, time period and HVSR based site class classifications of Lalitpur district. From our HVSR analysis zoning obtained for Lalitpur is for Stable zones (L-23, L-24) represent firm ground, less seismic amplification expected. Local amplification zones (L-3, L-7, L-13, L-14, L-21, L-19 (Figure 18)) are significant hazard due to high amplification (>2) and Instability zones (L-1, L-2, L-4, L-5, L-9, L-15, L-20, L-22, L-25) are prone to resonance and might be instability due to long predominant periods in very soft soil. Table 2 shows the location with predominant frequency, amplification factor, time period, and HVSR based site class of Lalitpur stations.

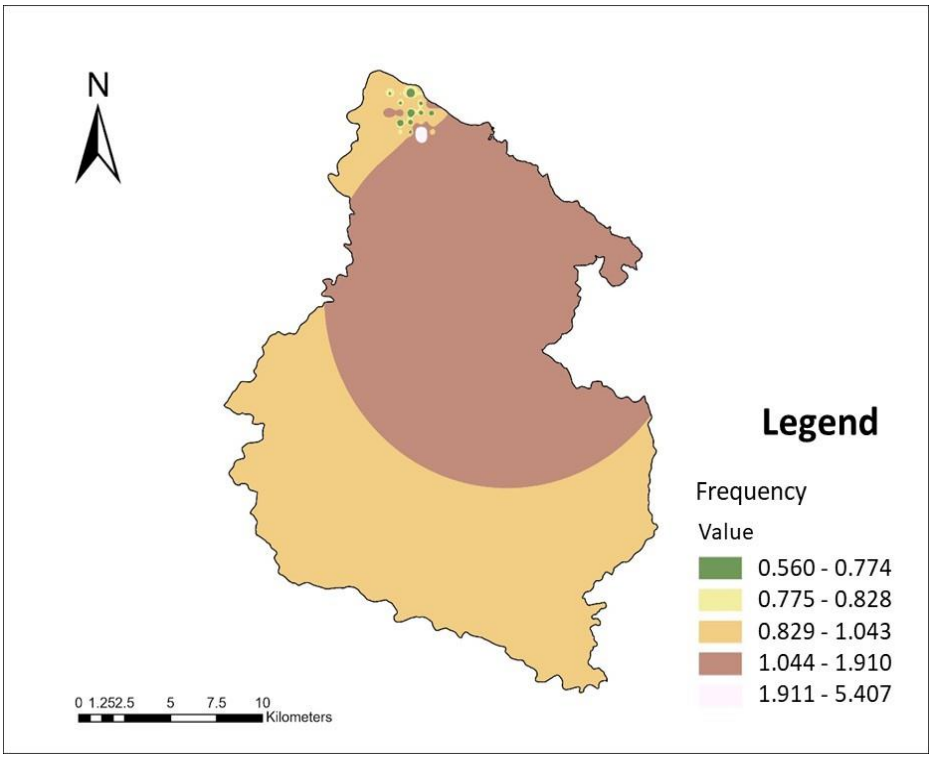


Figure 24. Predominant frequency zoning of core area of Lalitpur district

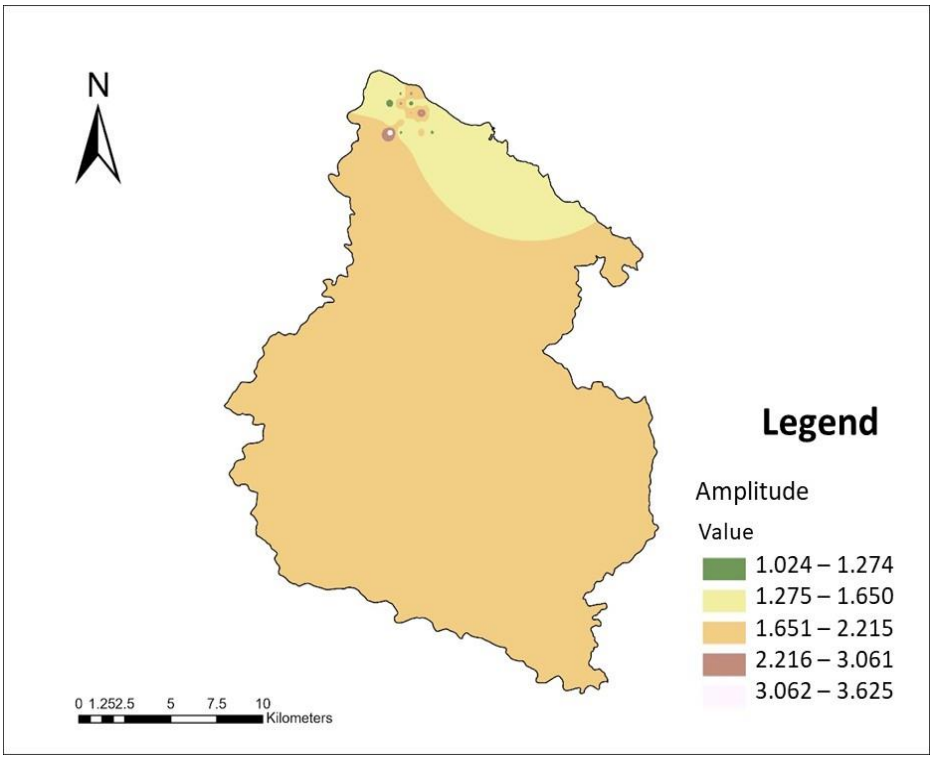


Figure 25. Amplification factor zoning of core area of Lalitpur district

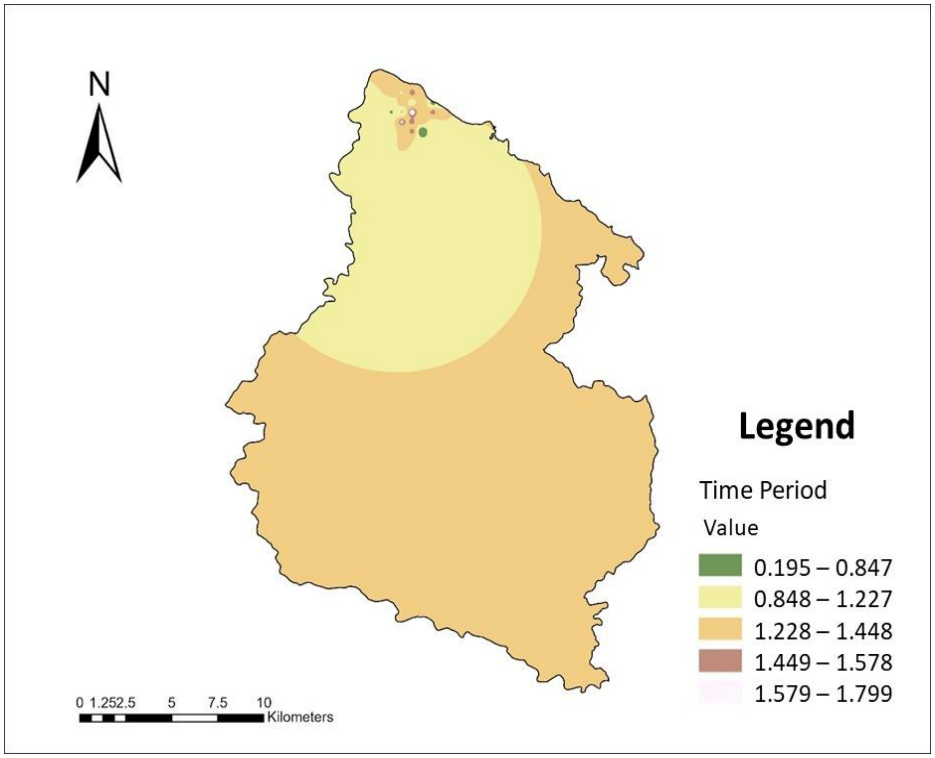


Figure 26. Time period zoning of core area of Lalitpur district

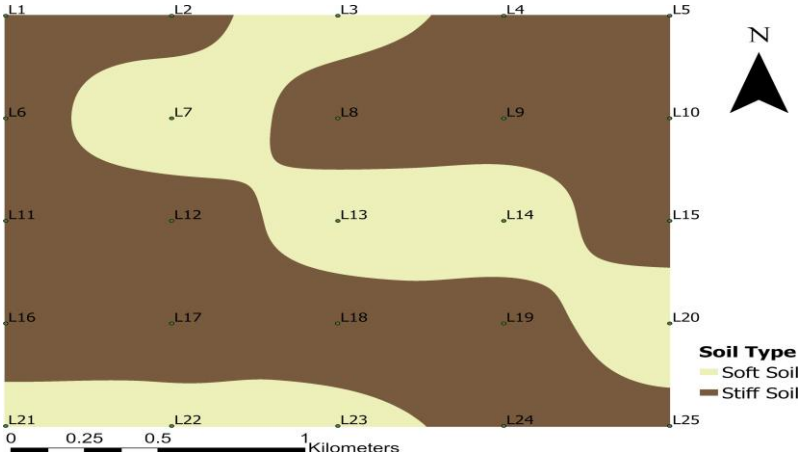


Figure 27. HVSR based site class Zoning of core area of Lalitpur district

Table 2 Predominant frequency, Amplification factor, Time period and HVSR based site class of Lalitpur Stations.

Station	Latitude	Longitude	Amplitude	Frequency (Hz)	Time period (Sec)	HVSR-based site class
L-1	27.6823940	85.3148620	1.2990	0.757	1.321	Stiff soil
L-2	27.6823940	85.3199410	1.2100	0.825	1.212	Stiff soil
L-3	27.6823940	85.3250194	2.3400	0.637	1.570	Soft Soil
L-4	27.6823940	85.3300980	1.8350	0.815	1.227	Stiff soil
L-5	27.6823940	85.3351760	1.6170	0.654	1.529	Stiff soil
L-6	27.6778970	85.3148630	1.0270	0.927	1.079	Stiff soil
L-7	27.6778970	85.3199410	2.3830	0.730	1.370	Soft Soil
L-8	27.6778970	85.3250194	1.0170	0.979	1.021	Stiff soil
L-9	27.6778970	85.3300980	1.3940	0.721	1.387	Stiff soil
L-10	27.6778970	85.3351760	1.4200	1.700	0.588	Stiff soil
L-11	27.6734000	85.3148630	1.3200	1.298	0.770	Stiff soil
L-12	27.6734000	85.3199410	1.3120	1.252	0.799	Stiff soil
L-13	27.6734000	85.3250194	2.2620	0.553	1.808	Soft Soil
L-14	27.6734000	85.3300970	3.1800	0.695	1.439	Soft Soil
L-15	27.6734000	85.3351760	1.4720	0.638	1.567	Stiff soil
L-16	27.6689030	85.3148630	1.2540	0.844	1.185	Stiff soil
L-17	27.6689030	85.3199410	1.7450	0.600	1.667	Stiff soil
L-18	27.6689030	85.3250190	1.2330	0.652	1.534	Stiff soil
L-19	27.6689030	85.3300970	1.5800	0.757	1.321	Stiff soil
L-20	27.6689030	85.3351750	1.2700	0.866	1.155	Stiff soil
L-21	27.6644060	85.3148640	3.6420	0.954	1.048	Soft Soil
L-22	27.6644060	85.3199420	1.1800	0.785	1.274	Stiff soil
L-23	27.6644060	85.3250194	1.4400	0.645	1.550	Stiff soil
L-24	27.6644060	85.3300970	1.7270	5.448	0.184	Stiff soil
L-25	27.6644060	85.3351750	1.2230	0.837	1.195	Stiff soil

(Soil Classification Based on Amplification (SESAME, 2004))

4.3 Free-Field Site Characteristics in Central Kathmandu

The predominant frequency of the microtremor observation point ranged from 0.436HZ to 3.976Hz, and the amplitude ranges from 1.05-3.28. Stations K-14, (Figure 27), K-14, K-15 and K-17 show soft soil, whereas other station soils are found to be Stiff soil. Station K-19, (Figure 26) and station K-22 (Figure 29) show samples of the HVSR graph with frequency, which represents the thick sediment deposits over the basement rock, which could result in the site's low frequency. Significantly higher frequencies with distinct HVSR curves (station K-14, Figure 27) are constituted by the basin's edges and some parts of the central region in the study area which might be an indication of shallow sediment deposits over the underlying bedrock. One borehole log data Point was considered, as illustrated in Figure 25, to validate the results. This verification shows that rocky sites or very thin sediment deposits are associated with high fundamental frequency, while thick sediment deposits (D'amico et al., 2004; Birgören et al., 2009; Paudyal et al. 2012). The lithological features of the borehole were classified based on the Unified Soil Classification System (USCS) adopted by ASTM (1996), as shown in Figure 33. BH-3 (Figure 34) and BH-4 (Figure 35) lie in the southern part (near station K-14) and comprise of shallow sediment deposits over the bedrock. Table 2 shows the location with predominant frequency, amplification factor, time-period, and HVSR based site class of Kathmandu stations.

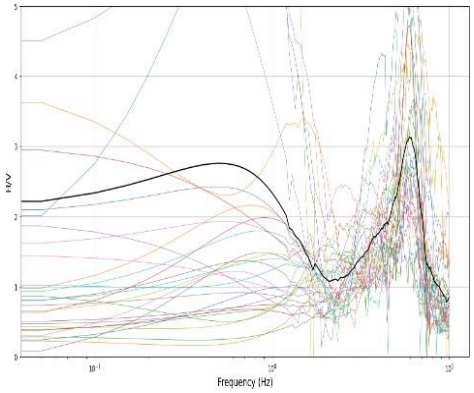


Figure 28. HVSR Plot of Station K-18

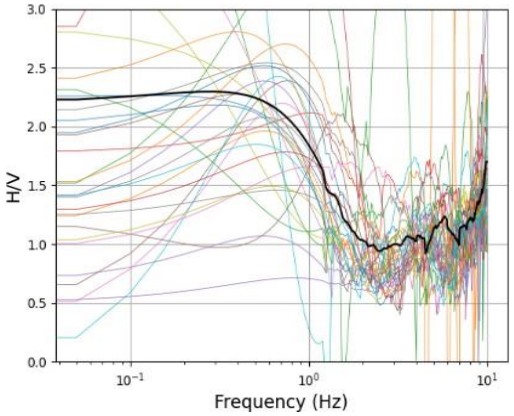


Figure 29. HVSR Plot of Station K-19

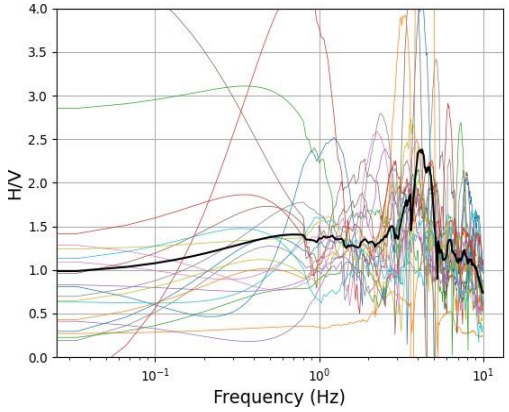


Figure 30. HVSR Plot of Station K-14

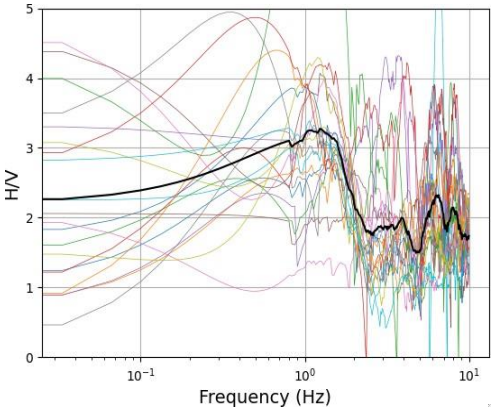


Figure 31. HVSR Plot of Station K-3

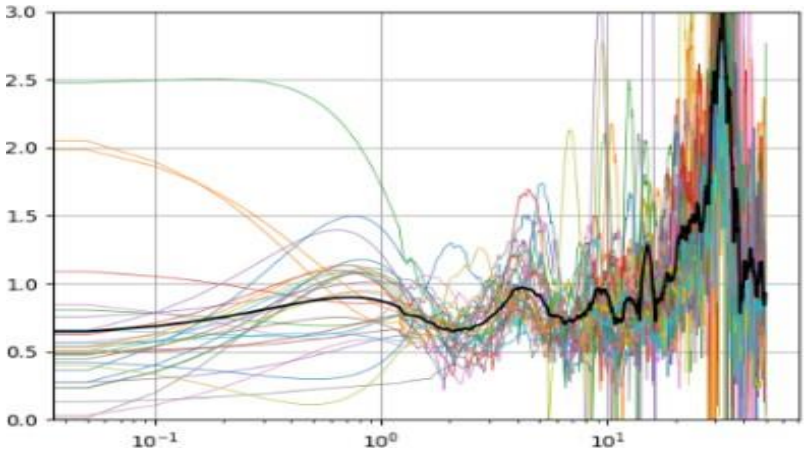


Figure 32. HVSR Plot of Station K-22

Table 3. Predominant frequency And Amplification factor of Kathmandu Stations

Station	Latitude	Longitude	Amplitude	Frequency (HZ)	Time period (Sec)	HVSR-based site class
K-1	27.710361	85.305859	0.945	1.578	0.634	Stiff soil
K-2	27.710361	85.310939	0.786	1.939	0.516	Stiff soil
K-3	27.710361	85.316019	0.899	3.286	0.304	Stiff soil
K-4	27.710361	85.321099	0.888	1.506	0.664	Stiff soil
K-5	27.710361	85.326179	0.688	1.496	0.668	Stiff soil
K-6	27.705864	85.30586	0.945	1.463	0.684	Stiff soil
K-7	27.705864	85.310939	0.925	1.104	0.906	Stiff soil
K-8	27.705864	85.316019	0.767	1.052	0.951	Stiff soil
K-9	27.705864	85.321099	0.562	1.211	0.826	Stiff soil
K-10	27.705864	85.326178	3.636	1.948	0.513	Soft Soil
K-11	27.701366	85.305861	0.767	1.589	0.629	Stiff soil
K-12	27.701367	85.31094	0.730	1.435	0.697	Stiff soil
K-13	27.7013667	85.316019	1.042	1.879	0.532	Stiff soil
K-14	27.701367	85.321099	3.976	1.929	0.518	Soft Soil
K-15	27.701366	85.326178	3.101	1.234	0.810	Soft Soil
K-16	27.696869	85.305862	0.695	1.240	0.806	Stiff soil
K-17	27.696869	85.310941	3.026	1.784	0.561	Stiff Soil
K-18	27.696869	85.31602	0.536	2.776	0.360	Stiff soil
K-19	27.696869	85.321099	0.436	2.280	0.439	Stiff soil
K-20	27.696869	85.326178	0.511	1.891	0.529	Stiff soil
K-21	27.692372	85.305861	0.796	1.238	0.808	Stiff soil
K-22	27.692372	85.31094	0.498	1.525	0.656	Stiff soil
K-23	27.692372	85.316019	0.592	1.638	0.611	Stiff soil
K-24	27.692372	85.321098	1.152	1.112	0.899	Stiff soil
K-25	27.692372	85.326177	0.888	1.420	0.704	Stiff soil

(Soil Classification Based on Amplification (SESAME,2004))

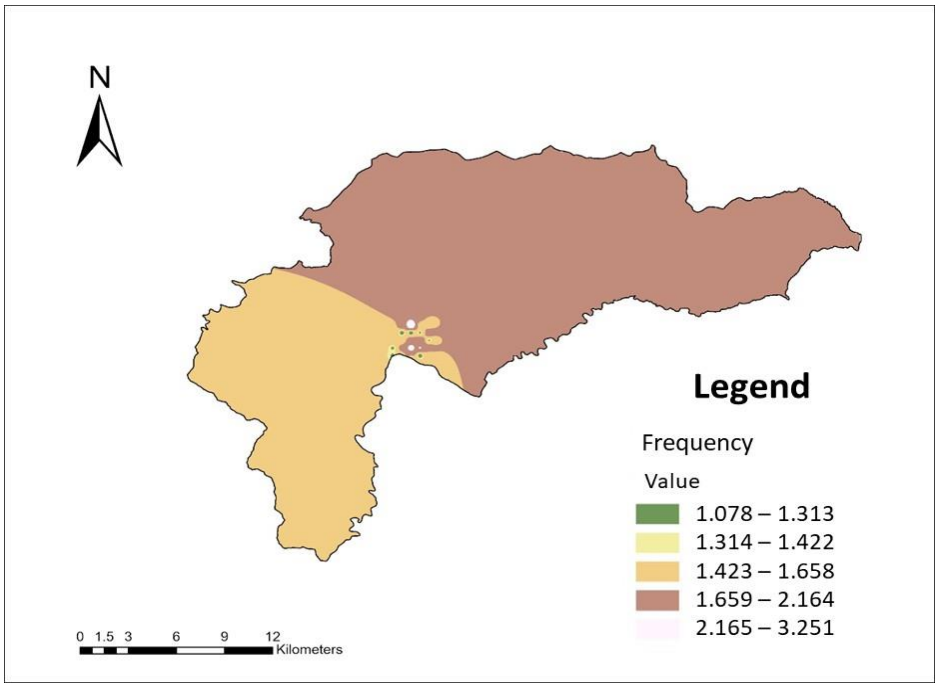


Figure 33. Predominant frequency zoning of core area of Kathmandu district

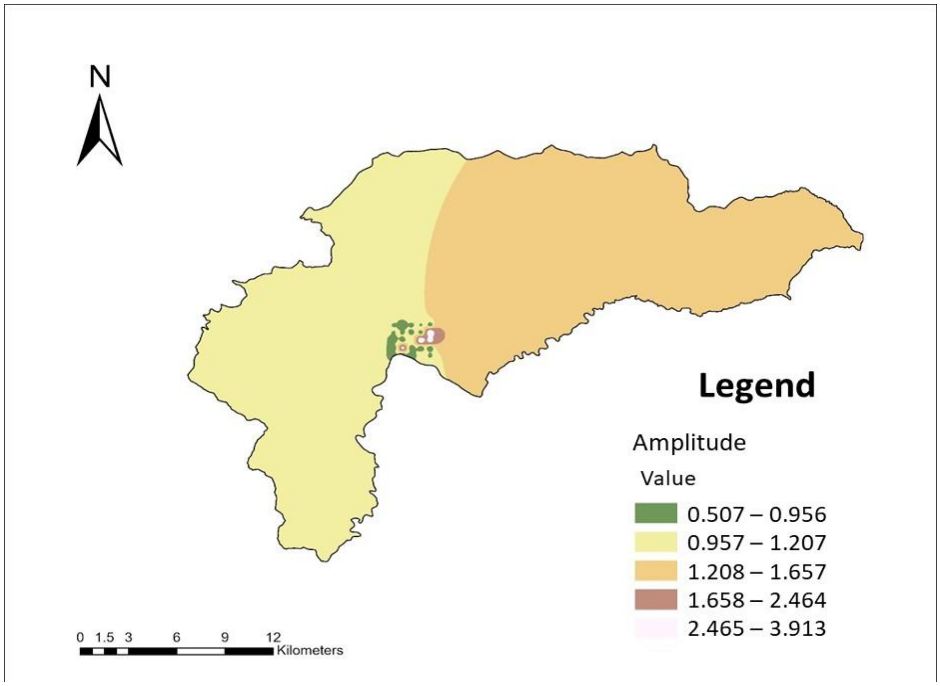


Figure 34. Amplification factor zoning of core area of Kathmandu district

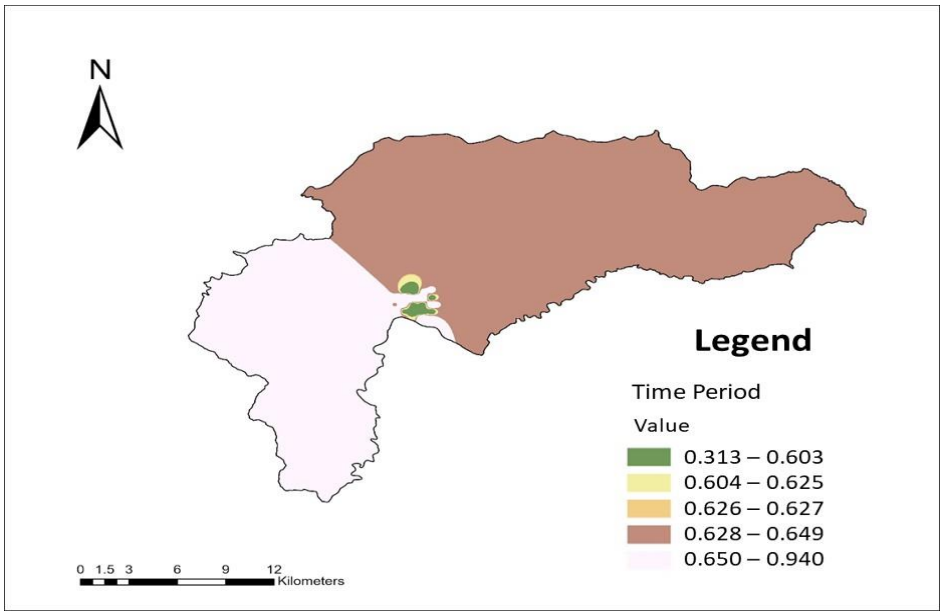


Figure 35. Time period zoning of core area of Kathmandu district

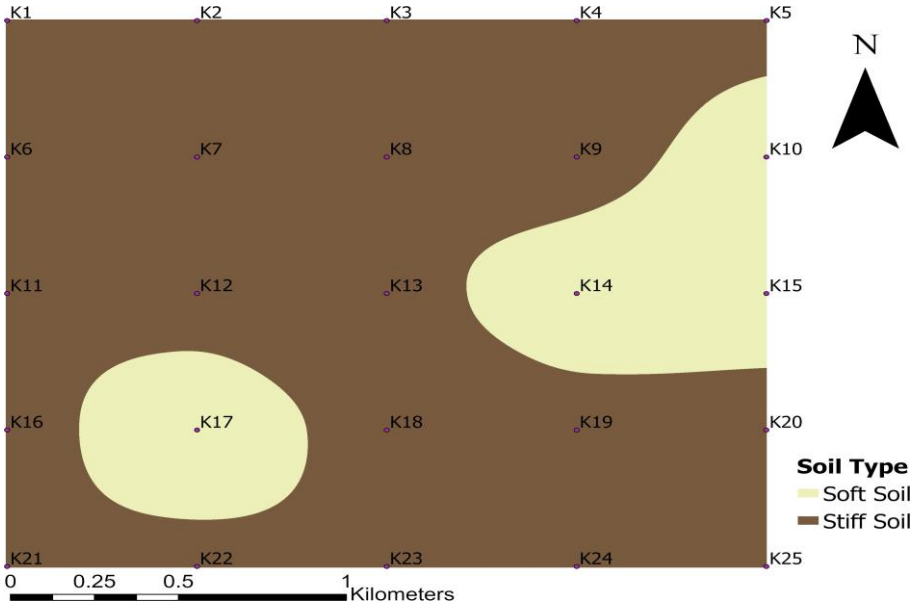


Figure 36. HVSR based site zoning of core area of Kathmandu district

Figure 30, Figure 31, Figure 32 and Figure 33 are zonation maps on a scale of 1:5,000 in terms of frequency, amplification, time-period and HVSR based site classifications of the Kathmandu district. We obtained zoning as stable zones from our HVSR analysis: K-3, K-18, K-19 represent relatively firm ground. Amplification-prone zones: K-10, K-14, K-15, and K-17 are highly susceptible to ground motion amplification and instability-prone zones: K-7, K-8, and K-9 have longer predominant periods and very soft soils indicate high seismic risk.

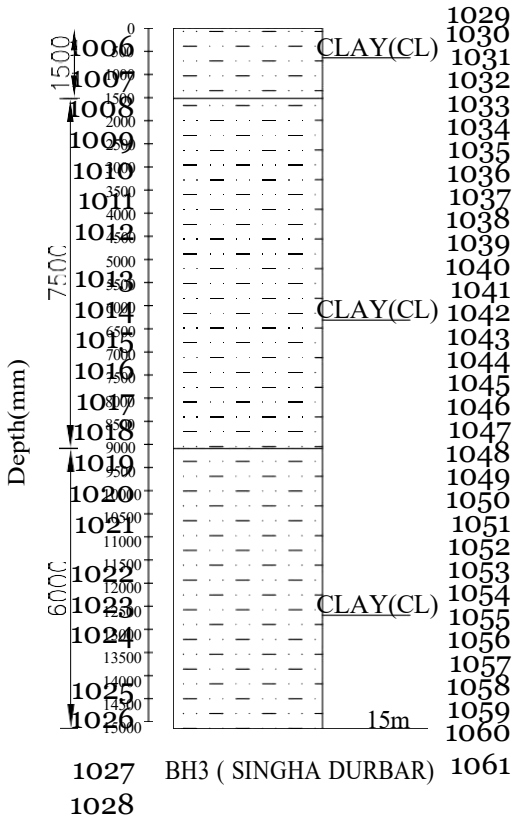


Fig. 37. Bore Hole BH 3-Singha durbar core area of Kathmandu district

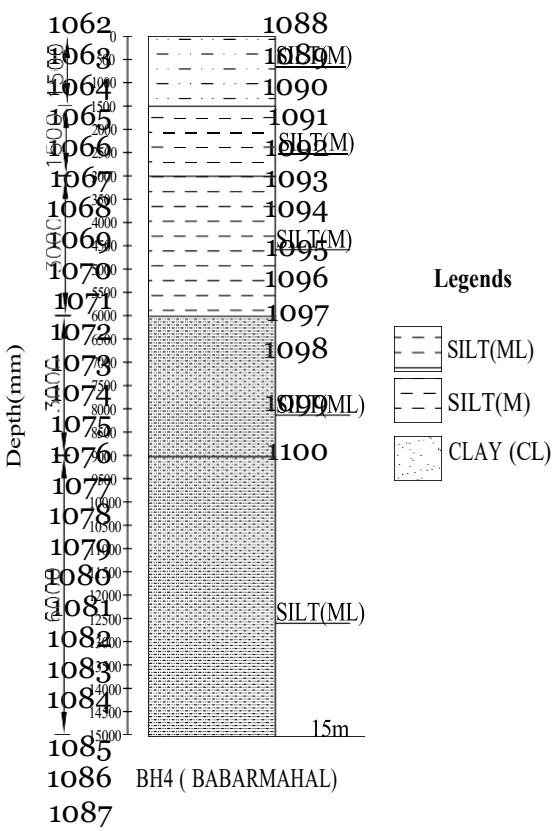


Fig. 38. Bore Hole BH 4-Babarmahal core area of Kathmandu district

Summarizing, Fp values ranged from 0.7 Hz in the deep lacustrine deposits of the northern valley to 6.5 Hz in the southern margins where shallow bedrock is present. The core areas of Kathmandu, Bhaktapur, and Lalitpur recorded Fp ranges of 0.44–3.98 Hz, 0.44–5.12 Hz, and 0.55–5.45 Hz, respectively. Higher frequencies were found along the basin edges, whereas lower values dominated in central Kathmandu. The Amplification factors (Ap) varied between 1.0 and 6.2. Notably, stations L-24 (Lalitpur) and B-21 (Bhaktapur) showed an Ap > 4.0, highlighting local zones of high seismic amplification. The mean Ap values for the core areas were Kathmandu, 1.05–3.28, Bhaktapur have 1.00–4.39, Lalitpur have 1.03–3.64. Based on Ap:1.3% of sites were classified as very soft soil (>=4), 24% as soft soil (2–4 Ap), 74.67% as stiff soil (<2). This classification indicates that the majority of Kathmandu Valley is dominated by stiff, soft, to very soft sediments, making it prone to amplification.

The microzonation map of the core area of Kathmandu Valley demonstrates that most of the northern part of the study region, which lies at a low elevation, has low-frequency content, which is due to the thick sediment deposits covering the bedrock. The southern and basin edges at higher elevations showed higher frequencies, which might be attributed to shallow sediment deposits over the bedrock. This implies that variations in elevation and uneven distribution of soil deposits alter the frequency of the ground; thus, topographical features, geological variations and non-uniform distribution of deposits have a considerable impact on the frequency of the site. However, topographic abnormalities, together with the focusing and diffraction phenomena of seismic waves and the nature of slopes may change the fundamental frequency of the site (Sanchez-Sesma 1987; Ashford et al. 1997; Falcone et al. 2023).

According to Paudyal et al. (2012), the fundamental frequency of soil deposits in the Kathmandu Basin ranges from 0.49-8.89 Hz. However, we found a slight increase in the frequency of deposits, which may have been caused by the shallow depth of rocks, extension of the study area to basin edges, and close spacing of station points. Paudyal et al. (2012) state that the

fundamental frequency of soil deposits in the Kathmandu basin ranges from 0.49 to 8.89 Hz likewise in our research we found free field frequency in the range of 0.436Hz to 5.558Hz which validates our research too. The shallow depth of rocks, extension of the study area to basin edges, and close spacing of station points, however, may be the causes of the minor increment in the frequency of deposits that we observed.

4.4 Seismic Risk Implications

Zones with both low frequency and high amplification (e.g., central Kathmandu, Bhaktapur core) represent the most critical hazard. Resonance effects are particularly concerning because many mid- to high-rise buildings in these zones have natural periods within the same range as soil frequencies. The results confirmed that structural vulnerability is amplified by local site effects.

4.5 Analytical Evaluation results

The Soil amplification Factor used many data from the reports already published and the Software Deepsoil. The error incorporated in these parameters are also reflected in the results so far obtained in this research work. Hence the obtained results may not represent the actual values for the region under consideration.

With the result obtained for soil amplification factor analysis of soil deposit of Kathmandu Valley, following conclusion are made.

1. In the most of the soil deposits, the amplification Factor ranges between 2 to 3 times.
2. From the result it is seen that, generally the amplification factor is higher towards southern deposit than the northern deposit.
3. The amplification factor is high in the soil deposits where the depth of clay is high in compare to other sand and gravel deposit.
4. The amplification of damped soil layer varies with the frequency content of the time history.
5. The amplification of soil deposits, increase with the increase of shear wave velocity of bedrock.

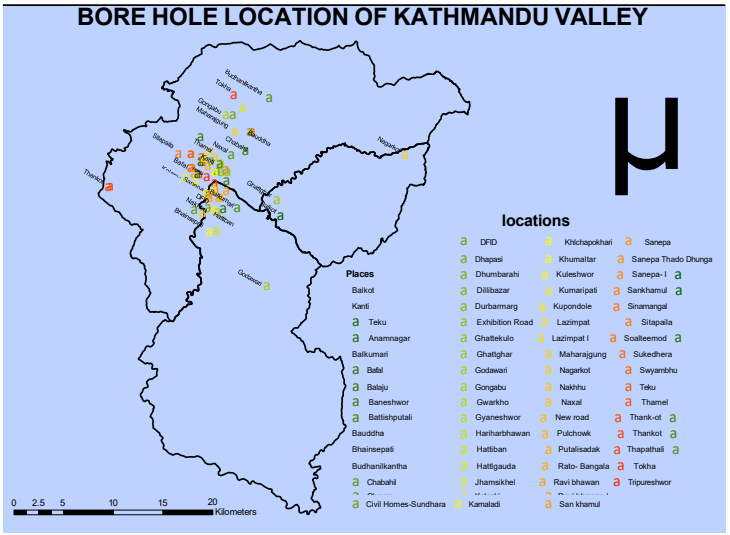


Fig.39 Bore hole location map of Kathmandu Valley

The figure shows a layered soil profile used in the one-dimensional site-response framework. 1-D analysis assumes approximately horizontal, laterally extensive layers and that the response is predominantly controlled by vertically propagating shear waves from the underlying bedrock.

Soil stiffness in the present analysis is represented using shear-wave velocity. The manuscript states that SPT-N values were converted to V_s using

$$V_s = 97N^{0.314}$$

(Ordóñez, 2006), and that a rigid bedrock condition with a very high shear-wave velocity was adopted. The DEEPSOIL framework is described as a 1-D equivalent-linear frequency-domain analysis capable of convolution and deconvolution.

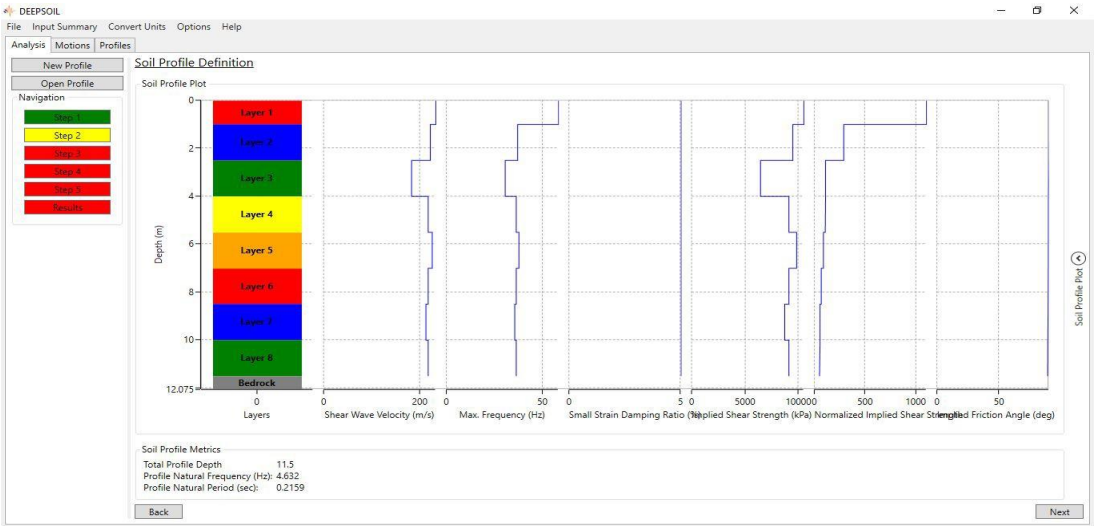


Fig.40 Soil Profile

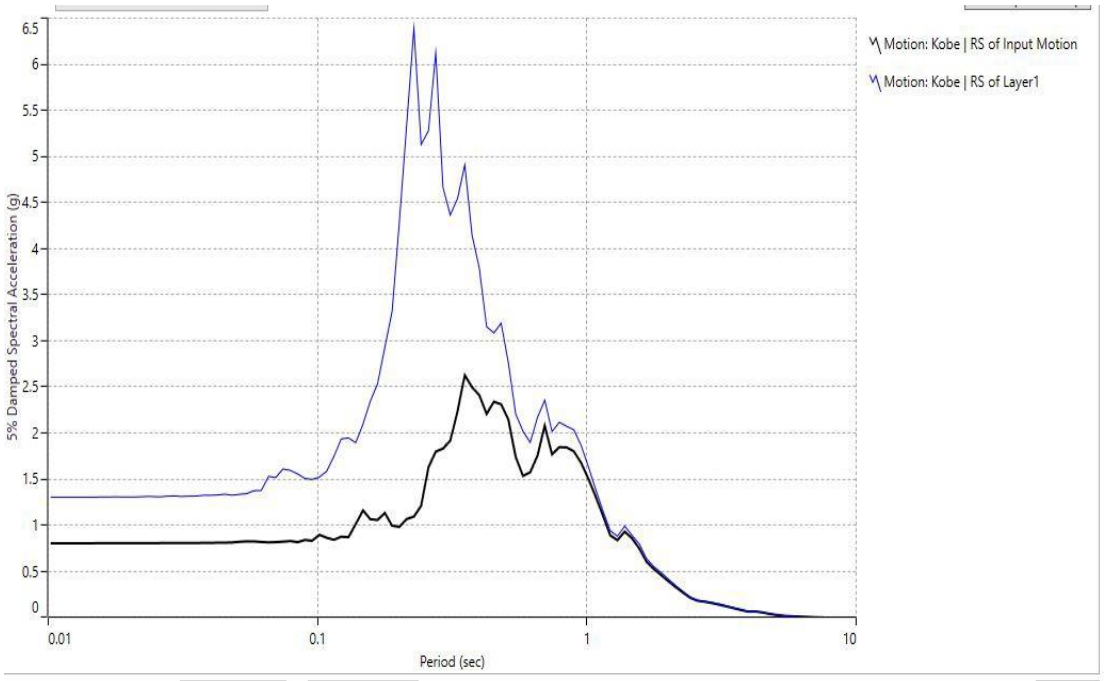


Fig.41 Response spectrum (Gangabu Eq Linear)

This response-spectrum figure represents the equivalent-linear analytical result for the Gangabu profile/input case shown in the manuscript. Equivalent-linear analysis represents the nonlinear behavior of soil approximately by using strain-compatible soil properties in an iterative

frequency-domain calculation. The plotted curve indicates how spectral acceleration changes with structural period after propagation through the modeled soil column. Peaks identify periods at which the modeled deposit can substantially modify the input motion. These peaks should be compared with the fundamental periods obtained from the microtremor/HVSR analysis and with the periods of structures of engineering interest.

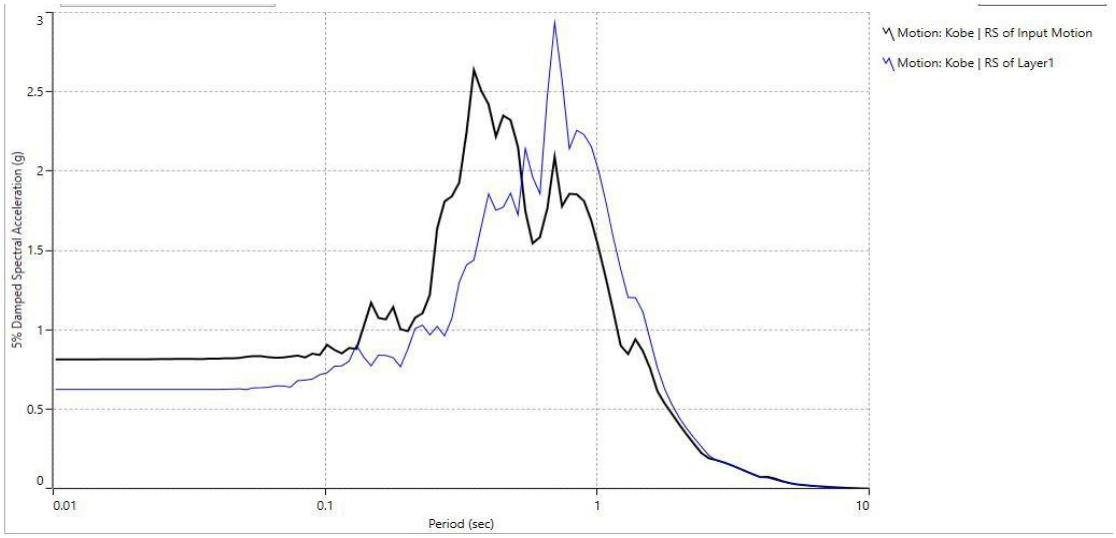


Fig.42 Response spectrum(Kathmandu District Non Linear)

This figure presents the nonlinear site-response result for the Kathmandu District case. Unlike an equivalent-linear approach, nonlinear time-domain analysis can update the stress–strain response directly as the motion progresses. The resulting spectrum therefore reflects the amplitude-dependent behavior of the soil more explicitly. The figure should be interpreted together with the soil profile and input motion: differences between equivalent-linear and nonlinear results can arise from modulus reduction, damping changes, and strain-dependent soil behavior.

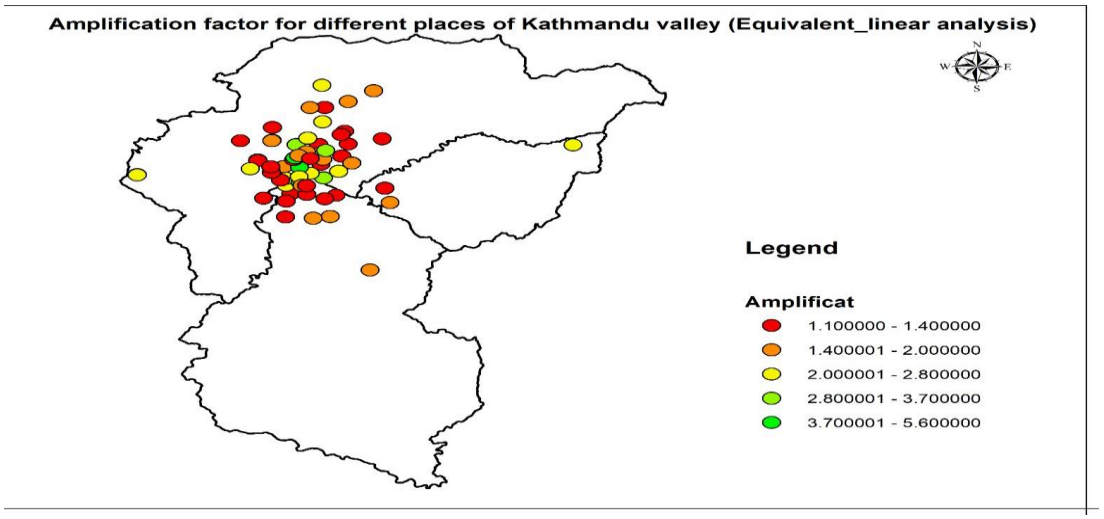


Fig43. Amplification Factor for Different Places of Kathmandu Valley (Equivalent Linear Analysis)

The map shows spatially varying amplification factors obtained from equivalent-linear site-response analysis. The legend indicates amplification classes from approximately 1.1 up to about

3.7 in the displayed results. Higher amplification values are concentrated in the central valley area, while lower values occur at more peripheral locations. This spatial pattern is consistent with the manuscript's interpretation that amplification is generally higher in southern/central deposits than in northern deposits and that thicker clay-rich deposits can produce greater amplification. The manuscript concludes that, for most soil deposits, amplification factors are commonly in the range of about 2–3 times.The nonlinear-analysis map shows the spatial distribution of amplification factors obtained from the nonlinear calculation. The displayed legend spans approximately 1.0 to 2.0, with the highest values concentrated mainly around the central cluster of investigated sites. Compared with the equivalent-linear map, the nonlinear results show a generally reduced amplification range. This is physically plausible because nonlinear soil behavior at higher strains can reduce stiffness and redistribute energy, limiting amplification at some frequencies. The comparison of Figures 43 and 44 is therefore valuable for assessing the sensitivity of predicted amplification to the selected constitutive/analysis approach.

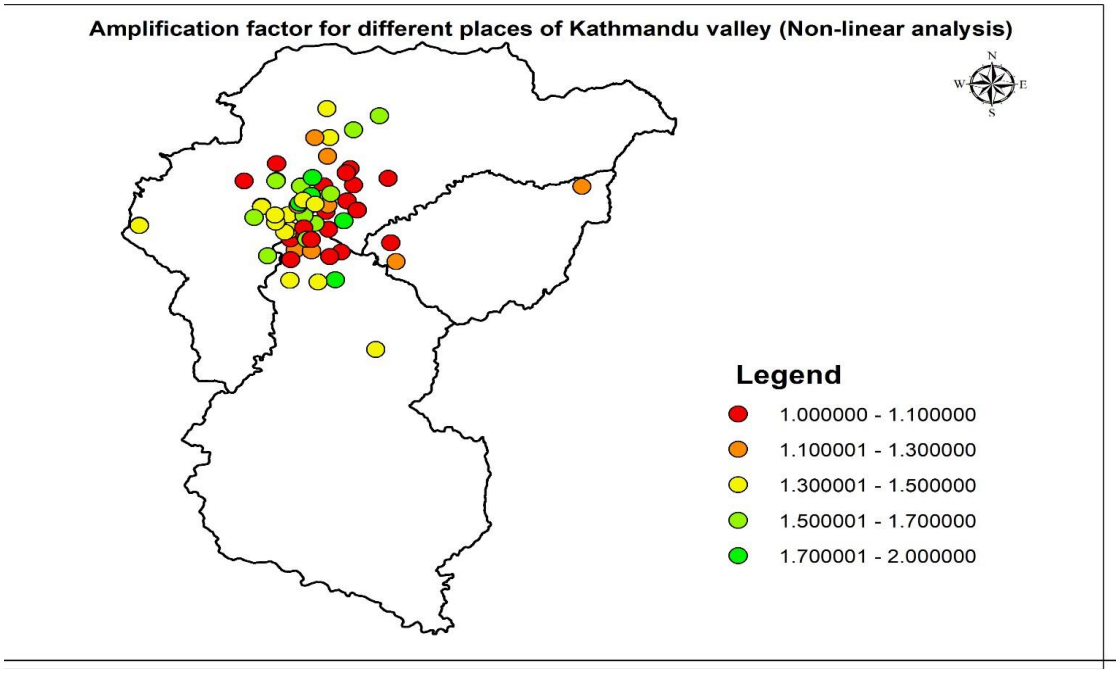


Fig 44. Amplification Factor for Different Places of Kathmandu Valley (Non-Linear Analysis)

4.6 Validations

Results obtained from microtremor measurement and available bore hole data at nearby station is compared

Table 4: Comparison of Microtremor results with Borehole Analysis

Stations	Measured frequency (microtremor)Hz	Borehole analysis frequency (Hz)	Validation
B21	3.592	4.667	ok
L24	5.448	4.294	ok
K10	3.636	3.912	ok
K14	3.976	3.995	ok

5 Conclusion

This study provides Priliminary seismic microzonation of the Kathmandu Valley using 75 single-station microtremor (HVSR) measurements. The predominant frequency (Fp) throughout the valley was between 0.7–5.45 Hz and the amplification factor (Ap) varied from 1.0–6.2. According to the amplification classification, 1.3 % of the sites were classified as very soft soils, 24 % as soft soils and 74.67 % as stiff soils. Lalitpur and Bhaktapur exhibited critical high-amplification sites (L-24 and B-21), which both coincided with densely populated areas with vulnerable building stock. The low frequency and high amplification combination in central Kathmandu further stresses the possibility of soil-structure resonance, which provides important data for earthquake hazard assessment, urban zoning, and seismic risk mitigation strategies. Although the HVSR in itself is not sufficient to completely quantify soil dynamics, it is a valuable first step in a valley-wide microzonation. Future studies should combine these results with shear wave velocity profiles, MASW surveys, and numerical basin response models. The obtained zones are stable zones, i.e. low maximum amplitude values (<1.5) show consistent ground response; similarly, the amplification prone zones in Bhaktapur have the highest amplification factor (4.39 at B-21) show strong resonance effects and the zones prone to instability in Lalitpur (L24) have the highest frequency (5.448Hz) show the possible risk of liquefaction or slope instability which needs to be confirmed with Vs profiling geotechnical data. The B-13 frequency (5.123 Hz) is the highest and is a characteristic of local heterogeneity. The study clearly shows the heterogeneity of Kathmandu Valley soils, which is often oversimplified in macro-scale hazard maps. The HVSR method yields reliable estimates of Fp and Ap, but for engineering applications, it should be supplemented by borehole Vs30 and MASW data. The selected spacing of 500 m $\times$ 500 m considerably enhanced the resolution of microzonation, allowing hazard assessment at the neighbourhood level. The results are in line with previous work but also give additional detailed information which might be useful for urban planning. The most pressing concern is soil-structure resonance, especially for mid-rise concrete buildings in central Kathmandu. This Study highlighted the need for site-specific building codes in Nepal. Data Limitations include ambient noise and lack of 2D/3D basin modelling. Nevertheless, this study provides a strong foundation for further hazard mapping and structural risk assessment.

Additionally, the spatial distribution of the Kathmandu Valley Soil Free-field frequency in the core aera of Kathmandu Valley was found to vary at in every station; therefore, this might be a useful tool for architects, engineers, and urban planners when they are first planning and designing projects. Therefore, the findings of this study offer valuable information on the geographical distribution of seismic risks, which is essential for risk assessment, efficient urban planning, and disaster mitigation techniques.

6 Acknowledgement

The authors thank several organizations for their assistance and data contributions. We are grateful to Khwopa College of Engineering for providing us with microtremor, and various soil test laboratory borehole data. The first author acknowledges that the Er. Sanjeeb Pudasaini, Er. Saroj Adhakari, Er. Chirag Pradhananga, Er. Dinesh Sakha Shrestha and Er. Unisha Ghimire for assistance received during the collection of field data and interpretation. Above all, I would like to thank my wife Er. Kundan Sharma for her constant motivation during my academic journey.

7 Authors' Contribution

All authors contributed to the conception and design of the study. Khemraj Pokharel, Ram Chandra Tiwari and Hari Ram Parajuli gathered information, produced the materials, and performed the analysis. The original draft of the manuscript was written by Khemraj Pokharel, with feedback from other authors on a pervious draft. All the authors have read and approved the final manuscript.

8 Funding

The authors declare that they have not received any funds or support for writing this work.

9 Data Availability

If the authors have access to data used in the study, they will make the data available.

10 Ethical Declarations

Conflict of interest: The writers are not required to declare any pertinent financial or non-financial interests.

References

[1] Acharya, P., Sharma, K., & Acharya, I. P. (2021). Seismic liquefaction risk assessment of critical facilities in Kathmandu Valley, Nepal. *GeoHazards*, 2(3), 153–171. https://doi.org/10.3390/geohazards2030009

[2] Ashford, S. A., Sitar, N., Lysmer, J., and Deng, N. (1997). Topographic effects on the seismic response of steep slopes. *Bulletin of the Seismological Society of America*, 87(3), 701–709.

[3] Ayers, R. L. and Bollinger, G. A. (1975). A study of microseismic and macroseismic ground motions in Virginia. *Pure and Applied Geophysics*, 113, 695–711.

[4] Bard, P. Y. (1998). Microtremor measurements: a tool for site effect estimation. In: *Proceedings of 2nd International Symposium on the Effect of Surface Geology on Seismic Motion*, Vol. III, Yokohama, Japan, pp. 1251–1279.

[5] Bijukchhen, S., Takai, N., Shigefuji, M., Ichiyanagi, M., and Sasatani, T. (2017). Strong-motion characteristics and visual damage assessment around seismic stations in Kathmandu after the 2015 Gorkha, Nepal, earthquake. *Earthquake Spectra*, 33(1_suppl), 219–242.

[6] Bijukchhen, S. M., Takai, N., Shigefuji, M., Ichiyanagi, M., Sasatani, T., and Sugimura, Y. (2017). Estimation of 1-D velocity models beneath strong-motion observation sites in the Kathmandu Valley using strong-motion records from moderate-sized earthquakes. *Earth, Planets and Space*, 69, 1–16.

[7] Bilham, R., Lodi, S., Hough, S., Bukhary, S., Khan, A. M., and Rafeeqi, S. F. A. (2008). Seismic hazard in Karachi, Pakistan: uncertain past, uncertain future.

[8] Birgören, G., Özel, O., and Siyahi, B. (2009). Bedrock depth mapping of the coast south of Istanbul: Comparison of analytical and experimental analyses. *Turkish Journal of Earth Sciences*, 18(2), 315–329. https://doi.org/10.3906/yer-0712-3

[9] Chamlagain, D. and Gautam, D. (2015). Seismic hazard in the Himalayan intermontane basins: an example from Kathmandu Valley, Nepal. In *Mountain Hazards and Disaster Risk Reduction*, pp. 73–103.

[10] Chamlagain, D. (2009). Earthquake scenario and recent efforts toward earthquake risk reduction in Nepal. *Journal of South Asia Disaster Studies*, 2(1), 57–80.

[11] Cressie, N. (1993). Statistics for Spatial Data (Revised Edition). *USA:John Wiley & Sons, Inc.,p.*.

[12] Chapagain, S. K., Pandey, V. P., Shrestha, S., Nakamura, T., and Kazama, F. (2010). Assessment of deep groundwater quality in Kathmandu Valley using multivariate statistical techniques. *Water, Air, & Soil Pollution*, 210, 277–288.

[13] Chaulagain, H., Rodrigues, H., Silva, V., Spacone, E., and Varum, H. (2016). Earthquake loss estimation for the Kathmandu Valley. *Bulletin of Earthquake Engineering*, 14, 59–88.

[14] D'Amico, V., Picozzi, M., Albarello, D., Naso, G., and Tropenscovino, S. (2004). Quick estimates of soft sediment thicknesses from ambient noise horizontal-to-vertical spectral ratios: a case study in southern Italy. *Journal of Earthquake Engineering*, 8(6), 895–908. https://doi.org/10.1080/13632460409350513

[15] Dangol, G. M. (1985). Geology of the Kathmandu fluviatile lacustrine sediments in the light of new vertebrate fossil occurrences. *Journal of Nepal Geological Society*, 3, 43–57.

[16] Falcone, G., Elia, G., and di Lernia, A. (2023). Investigating the influence of a pre-existing shear band on the seismic response of ideal step-like slopes subjected to weak motions: preliminary results. *Geosciences*, 13(5), 148.

[17] Gallipoli, M. R., Mucciarelli, M., Castro, R. R., Monachesi, G., and Contri, P. (2004). Structure, soil–structure response and effects of damage based on observations of horizontal-to-vertical spectral ratios of microtremors. *Soil Dynamics and Earthquake Engineering*, 24(6), 487–495.

[18] Gautam, D., de Magistris, F. S., and Fabbrocino, G. (2017). Soil liquefaction in Kathmandu valley due to 25 April 2015 Gorkha, Nepal earthquake. *Soil Dynamics and Earthquake Engineering*, 97, 37–47.

[19] Gautam, P. and Yoshida, M. (1988). On the secondary magnetization observed in the Nawakot Complex rocks, Malekhu area, Central Nepal. *Journal of Nepal Geological Society*, 5(1), 1–10.

[20] Geli, L., Cochran, J. R., Lee, T. C., Francheteau, J., Labails, C., Fouchet, C., and Christie, D. (2007). Thermal regime of the Southeast Indian Ridge between 88 E and 140 E: Remarks on the subsidence of the ridge flanks. *Journal of Geophysical Research: Solid Earth*, 112(B10).

[21] Gosar, A., Rošer, J., Šket Motnikar, B., and Zupančič, P. (2010). Microtremor study of site effects and soil-structure resonance in the city of Ljubljana (central Slovenia). *Bulletin of Earthquake Engineering*, 8(3), 571–592.

[22] Konno, K. and Ohmachi, T. (1998). Ground-motion characteristics estimated from spectral ratio between horizontal and vertical components of microtremor. *Bulletin of the Seismological Society of America*, 88(1), 228–241. https://doi.org/10.1785/bssa0880010228

[23] Lermo, J. and Chávez-García, F. J. (1993). Site effect evaluation using spectral ratios with only one station. *Bulletin of the Seismological Society of America*, 83(5), 1574–1594. https://doi.org/10.1785/bssa0830051574

[24] Mancini, F. E., Sánchez, M. A., Spagnotto, S., Alvarez, G., and Ahumada, F. (2024). Integration of airborne geophysical data for the characterization of the geothermal system in Valle del Cura, high central Andes. *Journal of South American Earth Sciences*, 149, 105203.

[25] Molnar, S., Sirohey, A., Assaf, J., Bard, P. Y., Castellaro, S., Cornou, C., and Yong, A. (2022). A review of the microtremor horizontal-to-vertical spectral ratio (MHVSR) method. *Journal of Seismology*, 26(4), 653–685.

[26] Nakamura, Y.(1989). A method for Dynamic characteristics Estimation of Subsurface Using Microtremor on the Ground Surface. In *Quarterly Report of RTRI,30,25-33*.

[27] Osorio, L. and Mayoral, J. M. (2013). Seismic microzonation for the northeast Texcoco lake area, Mexico. *Soil Dynamics and Earthquake Engineering*, 48, 252–266.

[28] Pamuk, E., Özdağ, Ö. C., Özyalın, Ş., and Akgün, M. (2017). Soil characterization of Tınaztepe region (Izmir/Turkey) using surface wave methods and Nakamura (HVSR) technique. *Earthquake Engineering and Engineering Vibration*, 16(2), 447–458. https://doi.org/10.1007/s11803-017-0392-y

[29] Pamuk, E., Özdağ, Ö. C., Tunçel, A., Özyalın, Ş., and Akgün, M. (2018). Local site effects evaluation for Aliağa/Izmir using HVSR (Nakamura technique) and MASW methods. *Natural Hazards*, 90, 887–899.

[30] Pandey, M. R. and Molnar, P. (1988). The distribution of intensity of the Bihar-Nepal earthquake of 15 January 1934 and bounds on the extent of the rupture zone. *Journal of Nepal Geological Society*, 5(1), 22–44.

[31] Pandey, M. R., Tandukar, R. P., Avouac, J. P., Vergne, J., and Heritier, T. (1999). Seismotectonics of the Nepal Himalaya from a local seismic network. *Journal of Asian Earth Sciences*, 17(5–6), 703–712.

[32] Panou, A. A., Theodulidis, N., Hatzidimitriou, P. M., Papazachos, C. B., and Stylianidis, K. (2004). Ambient noise horizontal-to-vertical spectral ratio for assessing site effects in urban environments: The case of Thessaloniki city (Northern Greece). *Bulletin of the Geological Society of Greece*, 36(3), 1467–1476.

[33] Paudyal, Y. R., Yatabe, R., Bhandary, N. P., and Dahal, R. K. (2012). A study of local amplification effect of soil layers on ground motion in the Kathmandu Valley using microtremor analysis. *Earthquake Engineering and Engineering Vibration*, 11, 257–268.

[34] Pegah, E. and Liu, H. (2016). Application of near-surface seismic refraction tomography and multichannel analysis of surface waves for geotechnical site characterizations: A case study. *Engineering Geology*, 208, 100–113.

[35] Pokharel, T. and Goldsworthy, H. M. (2017). Lessons learned from the Nepal earthquake 2015. *Australian Journal of Structural Engineering*, 18(1), 11–23. https://doi.org/10.1080/13287982.2017.1309818

[36] Sakai, H. (2001). Stratigraphic division and sedimentary facies of the Kathmandu Basin Group, central Nepal. *Journal of Nepal Geological Society*, 25, 19–32.

[37] Sakai, H. (2001). The Kathmandu Basin: an archive of Himalayan uplift and past monsoon climate. *Journal of Nepal Geological Society*, 25, 1–8.

[38] Sakhakarmi, D., Kawan, C. K., Prajapati, A., Pradhananga, C., Karanjit, S., and Bijukchhen, S. M. (2024). Seismic microzonation and soil-structure resonance analysis in Suryabinayak Municipality, Bhaktapur, Nepal: insights from ambient vibration measurements. *Geomatics, Natural Hazards and Risk*, 15(1), 2311892.

[39] Sánchez-Sesma, F., Chávez-Pérez, S., Suarez, M., Bravo, M. A., and Pérez-Rocha, L. E. (1988). The Mexico earthquake of September 19, 1985—On the seismic response of the Valley of Mexico. *Earthquake Spectra*, 4(3), 569–589.

[40] Sapkota, A., Sapkota, B., Poudel, J., and Giri, S. (2024). Comparative study on the seismic performance of a typical low-rise building in Nepal using different seismic codes. *Asian Journal of Civil Engineering*, 25(6), 4373–4394. https://doi.org/10.1007/s42107-024-01053-5

[41] Shepard,D. (1968). A Two-Dimensional Interpolation Function for Irregularly-Spaced Data. *Proceedings of the 1968 ACM National Conference, New York,27-29 August 1968*, 517-524. http://dx.doi.org/10.1145/800186.810616

[42] Sawada, S. (2004). A simplified equation to approximate natural period of layered ground on the elastic bedrock for seismic design of structures. In *Proceedings of the 13th World Conference on Earthquake Engineering*.

[43] Tuladhar, R., Yamazaki, F., Warnitchai, P., and Saita, J. (2004). Seismic microzonation of the greater Bangkok area using microtremor observations. *Earthquake Engineering & Structural Dynamics*, 33(2), 211–225.

[44] Willmott, C.J. and Matsuura, K. (2005). Advantages of the Mean Absolute Error(MAE) over the Root Mean Square Error (RMSE) in Assessing Average Performance. *Climate Research,30*, 33(2), 79-82. http://dx.doi.org/10.3354/cr030079

[45] Yong, A. (2007). *Geophysical site characterization using geomorphology, geology and integrated digital imaging methods on satellite data*. Doctoral dissertation, California State University, Northridge.

[46] Yulians, M., Tohari, A., and Rochman, J. P. G. N. (2024). Development of seismic microzonation for Rancaekek Sub-District using microtremor method. In *IOP Conference Series: Earth and Environmental Science*, 1373(1), 012017. IOP Publishing.